Article

Cell

Amino Acid Restriction Triggers Angiogenesis via GCN2/ATF4 Regulation of VEGF and H_2S Production

Graphical Abstract

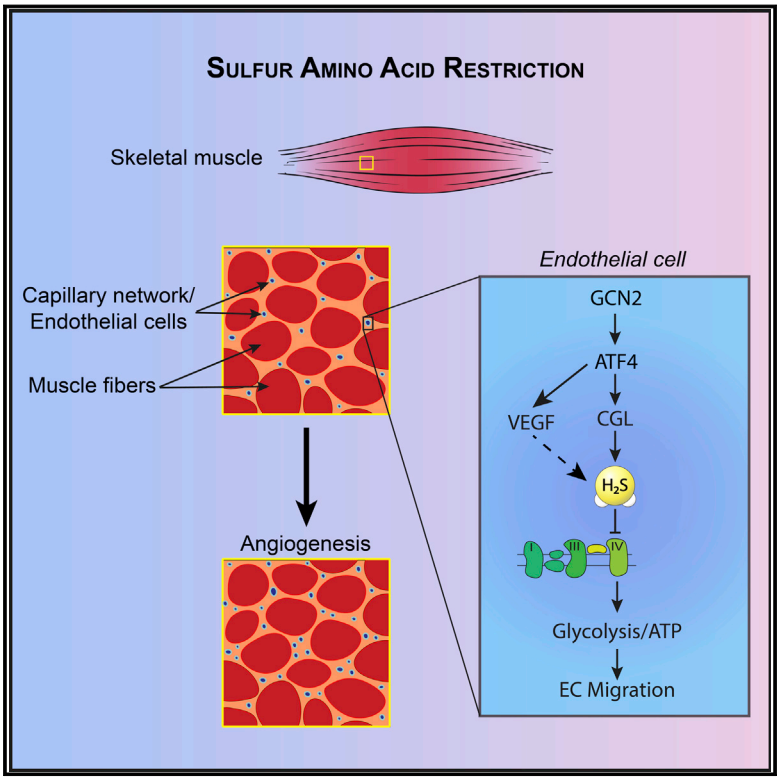

Highlights

- Sulfur amino acid (SAA) restriction triggers angiogenesis independent of hypoxia or HIF1α
- GCN2/ATF4 pathway regulates VEGF and CGL expression upon SAA restriction in ECs
- CGL is required for skeletal muscle angiogenesis activated by diet or exercise
- H_2S triggers glucose uptake, glycolysis, and PPP concomitant with OXPHOS inhibition in ECs

Authors

Alban Longchamp, Teodelinda Mirabella, Alessandro Arduini, ..., Christopher S. Chen, C. Keith Ozaki, James R. Mitchell

Correspondence

jmitchel@hsph.harvard.edu

In Brief

Restricting dietary sulfur amino acids can trigger angiogenesis and improve vascular health.

Longchamp et al., 2018, Cell *173*, 117–129
March 22, 2018
https://doi.org/10.1016/j.cell.2018.03.001

CellPress

Cell

Amino Acid Restriction Triggers Angiogenesis via GCN2/ATF4 Regulation of VEGF and H_2S Production

Alban Longchamp,[1,2,10] Teodelinda Mirabella,[3,4,10] Alessandro Arduini,[1,10] Michael R. MacArthur,[1] Abhirup Das,[5,6] J. Humberto Treviño-Villarreal,[1] Christopher Hine,[1] Issam Ben-Sahra,[1] Nelson H. Knudsen,[1] Lear E. Brace,[1] Justin Reynolds,[1] Pedro Mejia,[1] Ming Tao,[2] Gaurav Sharma,[2] Rui Wang,[7] Jean-Marc Corpataux,[8] Jacques-Antoine Haefliger,[8] Kyo Han Ahn,[9] Chih-Hao Lee,[1] Brendan D. Manning,[1] David A. Sinclair,[5,6] Christopher S. Chen,[3,4] C. Keith Ozaki,[2] and James R. Mitchell[1,11,*]

[1]Department of Genetics and Complex Diseases, Harvard T.H. Chan School of Public Health, Boston, MA, USA
[2]Department of Surgery and the Heart and Vascular Center, Brigham & Women's Hospital and Harvard Medical School, Boston, MA, USA
[3]Tissue Microfabrication Lab, Department of Biomedical Engineering, Boston University, Boston, MA, USA
[4]Wyss Institute for Biologically Inspired Engineering, Boston, MA, USA
[5]Glenn Center for the Biological Mechanisms of Aging, Department of Genetics, Harvard Medical School, Boston, MA 02115, USA
[6]Laboratory for Ageing Research, Department of Pharmacology, School of Medical Sciences, University of New South Wales, Sydney NSW 2052, Australia
[7]Cardiovascular and Metabolic Research Unit, Laurentian University, Sudbury, ON, Canada
[8]Department of Vascular Surgery, Laboratory of Experimental Medicine, Centre Hospitalier Universitaire Vaudois, Lausanne, Switzerland
[9]Department of Chemistry, Postech, 77 Cheongam-Ro, Nam-Gu, Pohang, 37673, Republic of Korea
[10]These authors contributed equally
[11]Lead Contact
*Correspondence: jmitchel@hsph.harvard.edu
https://doi.org/10.1016/j.cell.2018.03.001

SUMMARY

Angiogenesis, the formation of new blood vessels by endothelial cells (ECs), is an adaptive response to oxygen/nutrient deprivation orchestrated by vascular endothelial growth factor (VEGF) upon ischemia or exercise. Hypoxia is the best-understood trigger of VEGF expression via the transcription factor HIF1α. Nutrient deprivation is inseparable from hypoxia during ischemia, yet its role in angiogenesis is poorly characterized. Here, we identified sulfur amino acid restriction as a proangiogenic trigger, promoting increased VEGF expression, migration and sprouting in ECs *in vitro*, and increased capillary density in mouse skeletal muscle *in vivo* via the GCN2/ATF4 amino acid starvation response pathway independent of hypoxia or HIF1α. We also identified a requirement for cystathionine-γ-lyase in VEGF-dependent angiogenesis via increased hydrogen sulfide (H_2S) production. H_2S mediated its proangiogenic effects in part by inhibiting mitochondrial electron transport and oxidative phosphorylation, resulting in increased glucose uptake and glycolytic ATP production.

INTRODUCTION

Angiogenesis is the formation of new blood vessels from existing ones through sprouting, proliferation, and migration of endothelial cells (ECs). In adult mammals, angiogenesis is an adaptive response to normal and pathophysiological conditions characterized by inadequate supply of oxygen and nutrients, ranging from tissue ischemia upon vessel occlusion or tumorigenesis to endurance exercise.

Hypoxia is the best-understood trigger of angiogenesis, stabilizing the oxygen-sensitive transcription factor hypoxia-inducible factor (HIF)1α in multiple cell types and promoting expression of the master regulator of angiogenesis, vascular endothelial growth factor (VEGF). VEGF expression can also be induced by the transcriptional co-activator PGC1α upon nutrient deprivation through an ERR-α-dependent, HIF1α-independent pathway in muscle cells but not ECs (Arany et al., 2008), as well as by the ATF4 transcription factor downstream of the integrated stress response (ISR) triggered by either endoplasmic reticulum (ER) stress or amino acid (AA) deprivation (Abcouwer et al., 2002).

VEGF acts on ECs via binding to the cell-surface tyrosine kinase receptor VEGFR2, triggering an orchestrated cascade of signal transduction via the PI3K and mitogen-activated protein kinase (MAPK) pathways involving critical second messengers nitric oxide (NO) and cyclic guanosine monophosphate (cGMP) and changes in gene expression facilitating EC migration, proliferation, and vessel formation (Olsson et al., 2006). VEGF-mediated angiogenesis is potentiated by the NAD+-dependent deacetylase SIRT1, which deacetylates and inactivates FOXO transcription factors (Potente et al., 2007) involved in negative regulation of EC migration and tube formation (Potente et al., 2005). VEGF signaling also triggers changes in cellular energy metabolism—namely increased glucose uptake and glycolysis necessary to provide rapid energy for EC migration (De Bock et al., 2013).

Hydrogen sulfide (H_2S) is a proangiogenic gas (Cai et al., 2007; Szabó, 2007) produced in ECs upon VEGF stimulation (Papapetropoulos et al., 2009) primarily by the transsulfuration enzyme cystathionine-γ-lyase (CGL, a.k.a. CTH or CSE) (Wang, 2012). Like NO, which—in addition to activating cGMP synthesis—functions through post-translational modification (S-nitrosylation) of target proteins (Fukumura et al., 2006), H_2S promotes angiogenesis through S-sulfhydration and activation of proximal signal transduction components, including VEGFR2 (Tao et al., 2013) and endothelial nitric oxide synthase (eNOS) (Altaany et al., 2014; Coletta et al., 2012). Angiogenesis is compromised upon genetic CGL deficiency in aorta explant assays *ex vivo* (Papapetropoulos et al., 2009) and arterial ligation *in vivo* (Kolluru et al., 2015). However, mechanisms of CGL regulation in ECs and the relative contribution of H_2S versus NO in angiogenesis remain unclear (Katsouda et al., 2016).

Dietary restriction (DR), defined as reduced nutrient/energy intake without malnutrition, is best known for its ability to extend lifespan, improve metabolic fitness, and increase stress resistance (Colman et al., 2009; Fontana et al., 2010; Hine et al., 2015). DR regimens, which vary widely, can emphasize either restriction of total food intake (calorie restriction, CR) or dilution of specific nutrients in the diet, such as the sulfur AAs (SAAs) methionine (M) and cysteine (C) (M restriction, MR) (Miller et al., 2005; Orentreich et al., 1993). We recently reported that CR increases hepatic CGL expression, endogenous H_2S production capacity, and resistance to hepatic ischemia reperfusion injury, each of which is abrogated by dietary C supplementation (Hine et al., 2015). CR also promotes revascularization and recovery from femoral artery ligation in rodents (Kondo et al., 2009) and maintains vascular health in rodents and non-human primates in part by preserving capillary density in skeletal muscle (Omodei and Fontana, 2011). Interestingly, SIRT1 is activated in some tissues upon DR (Cantó and Auwerx, 2009; Wang, 2014) and required for VEGF-dependent angiogenesis (Potente et al., 2007). However, the effects of DR on angiogenesis and the potential role of H_2S remain unknown. Here, we identified SAA restriction as a proangiogenic trigger in ECs *in vitro* and in skeletal muscle in mice *in vivo*.

RESULTS

SAA Restriction Induces Endothelial VEGF Expression *In Vitro* and Functional Angiogenesis *In Vivo*

We tested the potential of isolated nutrient restriction independent of ischemia or hypoxia to impact angiogenesis *in vitro* using a model of SAA restriction (Hine et al., 2015). Human umbilical vein ECs (HUVECs) cultured overnight in media lacking SAAs (−M&C) displayed increased VEGF mRNA expression and protein secretion into the media (Figure 1A). This correlated with increased proangiogenic potential, including migration across a scratch (Figure 1B), formation of capillary-like structures (tube formation; Figure 1C), and increased sprout length in three-dimensional HUVEC spheroid cultures—an effect that was abrogated by the specific VEGFR2 inhibitor SU5416 (Figure 1D). Inhibiting SIRT1 activity with Ex-527 significantly reduced HUVEC tube formation (Figure 1C) and branch point number (Figure S1A) upon −M&C, suggesting that the proangiogenic pathway triggered by −M&C is dependent on both VEGF and SIRT1 activity.

To test the impact of dietary SAA restriction on angiogenesis *in vivo*, mice were given *ad libitum* access to an MR diet containing a limiting amount of M and lacking C (Miller et al., 2005; Orentreich et al., 1993). Young adult wild-type (WT) mice on MR for up to 2 months maintained a lower body weight despite normal food intake relative to mice fed a control diet containing normal M and C levels (Figure S1B).

Strikingly, MR resulted in increased vascular density in skeletal muscle as determined by immunohistochemistry (IHC) (Figure 1E) and flow cytometric analysis (Figure S1C) for the EC marker CD31. Consistent with VEGF dependence, this effect was blocked by axitinib, one of the best-characterized VEGF receptor inhibitors *in vivo* with demonstrated antiangiogenic activity in the context of tumor neovascularization (Ma and Waxman, 2008) (Figures 1E and S1C). Interestingly, although expression of VEGF mRNA was not consistently affected upon MR in whole gastrocnemius muscle (Figure S1D), there was a trend toward increased VEGF protein in gastrocnemius muscle extracts (Figure S1E). VEGF and CD31 co-localized in gastrocnemius muscle by IHC (Figure S1F), consistent with ECs as the source of VEGF upon MR *in vivo* as observed upon −M&C *in vitro* (Figure 1A).

Functional significance was tested in the context of femoral artery ligation in mice preconditioned on MR or control diet for 1 month prior to surgical occlusion and returned to a complete diet after surgery (Figure S1G). Although blood flow was similarly interrupted in both diet groups immediately after ligation (d0), return of blood flow indicative of neovascularization was accelerated in MR mice, with significant improvement by d3 after ligation (Figure 1F). CD31 IHC of muscle sections confirmed a relative increase in capillary density in both ischemic and non-ischemic legs of MR versus control mice despite a return to a complete diet for 10 days (Figure 1G). Functional improvement was also observed in mice preconditioned on a different DR regimen—40% CR—for 1 month prior to femoral ligation (Figures S1H and S1I). In addition to improved return of blood flow (Figure S1H), CR mice demonstrated improved treadmill exercise endurance testing on d4 after ligation (Figure S1I). Together, these data suggest neovascularization induced by DR (in the form of CR or MR) as a contributing factor in the improved physiological response to acute blood flow cessation.

GCN2-Dependent, Hypoxia-Independent Regulation of VEGF and Angiogenesis upon SAA Restriction

Although HIF1α upon hypoxia is the best-characterized trigger of VEGF expression in multiple cell types, including ECs, increased VEGF expression upon −M&C was unaffected by HIF1α RNAi knockdown (KD) (Figures 2A and S2A) and coincided with a trend toward reduced HIF1α protein expression (Figures 2B and S2B). PGC1α can also induce VEGF independently of HIF1α upon total nutrient/growth-factor deprivation in myocytes but not ECs (Arany et al., 2008). Consistent with this, endogenous PGC1α mRNA expression in HUVECs was very low as judged by Ct value (data not shown) and unaffected by −M&C (Figure S2C), while exogenous PGC1α

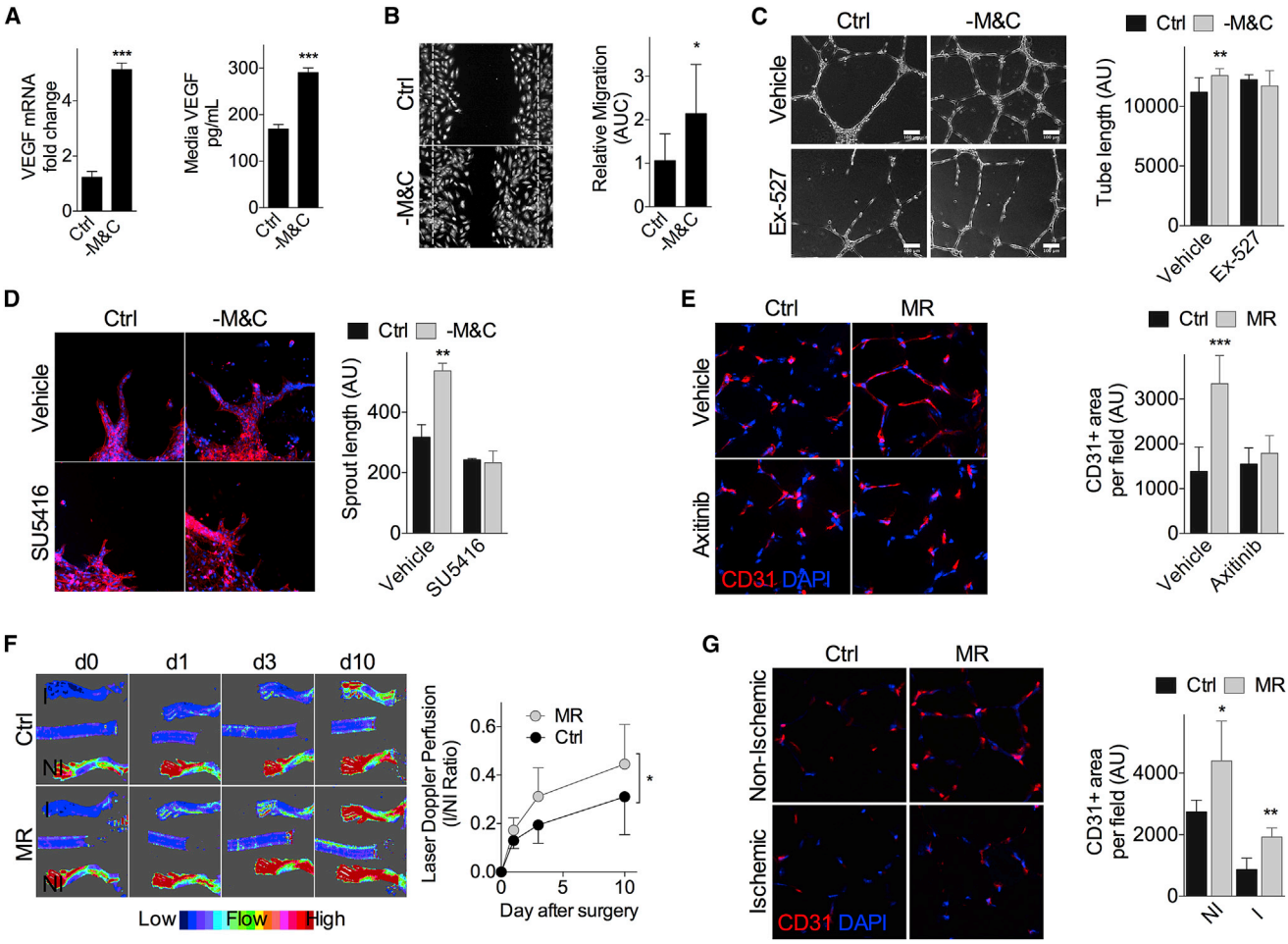

Figure 1. SAA Restriction Induces Endothelial VEGF Expression *In Vitro* and Functional Angiogenesis *In Vivo*

(A) VEGF mRNA levels (left, n = 4 experiments per group) and secreted protein concentration in the media (right, n = 6 experiments per group) of HUVECs cultured in control (Ctrl) or SAA-deficient (−M&C) media for 16 hr. Error bars indicate SEM.

(B) Migration assay: representative migration across a scratch (left, 10× magnification at t = 20 hr; dotted lines indicate boundary of the scratch at t = 0 hr) and area under the curve (AUC; right, n = 7–10 data points per condition, with each data point representing the mean of multiple measures within a single well in a representative experiment) from HUVECs cultured in the indicated media.

(C) Tube formation assay: representative capillary-like structures (left, 40× magnification) and quantification of tube length/field in arbitrary units (AU; right, n = 8–10 data points per condition) in HUVECs incubated in the indicated media ± SIRT1 inhibitor Ex-527 for 18 hr.

(D) Spheroid assay: representative images (left, 40× magnification) and quantification (right, in triplicate) of sprouting HUVEC spheroids in the indicated media ± VEGFR2 inhibitor SU5416 for 24 hr. Blue, DNA (DAPI); red, F-actin (phalloidin).

(E) Representative transverse sections (left, 40× magnification) and quantification (right) of gastrocnemius muscle stained for endothelial marker CD31 in mice fed for 2 weeks on control or MR diet ± VEGFR2 inhibitor axitinib; n = 6–8 mice per group.

(F) Longitudinal Doppler imaging of blood flow in WT mice preconditioned for 1 month on control or MR diet prior to femoral artery ligation (I, ischemic; NI, non-ischemic). Representative infrared images on the indicated day after ligation (left). Quantification of blood flow recovery with individual animal AUCs used for statistical comparison (right, n = 7–8 mice per group).

(G) Representative transverse sections (left, 40× magnification) and quantification (right) of CD31-stained gastrocnemius muscle 10 days after ligation from (F); n = 4 mice per group.

Error bars indicate SD unless otherwise noted; asterisks indicate the significance of the difference by Student's t test or one-way ANOVA with Sidak's multiple comparisons test between diets *in vivo* or SAA deprivation *in vitro*; *p < 0.05, **p < 0.01, ***p < 0.001. See also Figure S1.

overexpression in HUVECs failed to modulate VEGF expression (Figures S2D and S2E).

The AA starvation response (AASR), a branch of the ISR involving binding of uncharged cognate tRNAs to the general control nonderepressible 2 (GCN2) kinase, phosphorylation of eukaryotic translation initiation factor 2α (eIF2α), and translational derepression of ATF4 (Kilberg et al., 2005; Wek et al., 1995), has been implicated in DR-mediated resistance to ischemia reperfusion injury (Peng et al., 2012) but has not been assessed in ECs. In HUVECs, −M&C increased eIF2α phosphorylation, ATF4 protein expression, and transcription of the ATF4 target, Asns (Figures 2B, S2B, and S2F). ATF4 small interfering RNA (siRNA) reduced

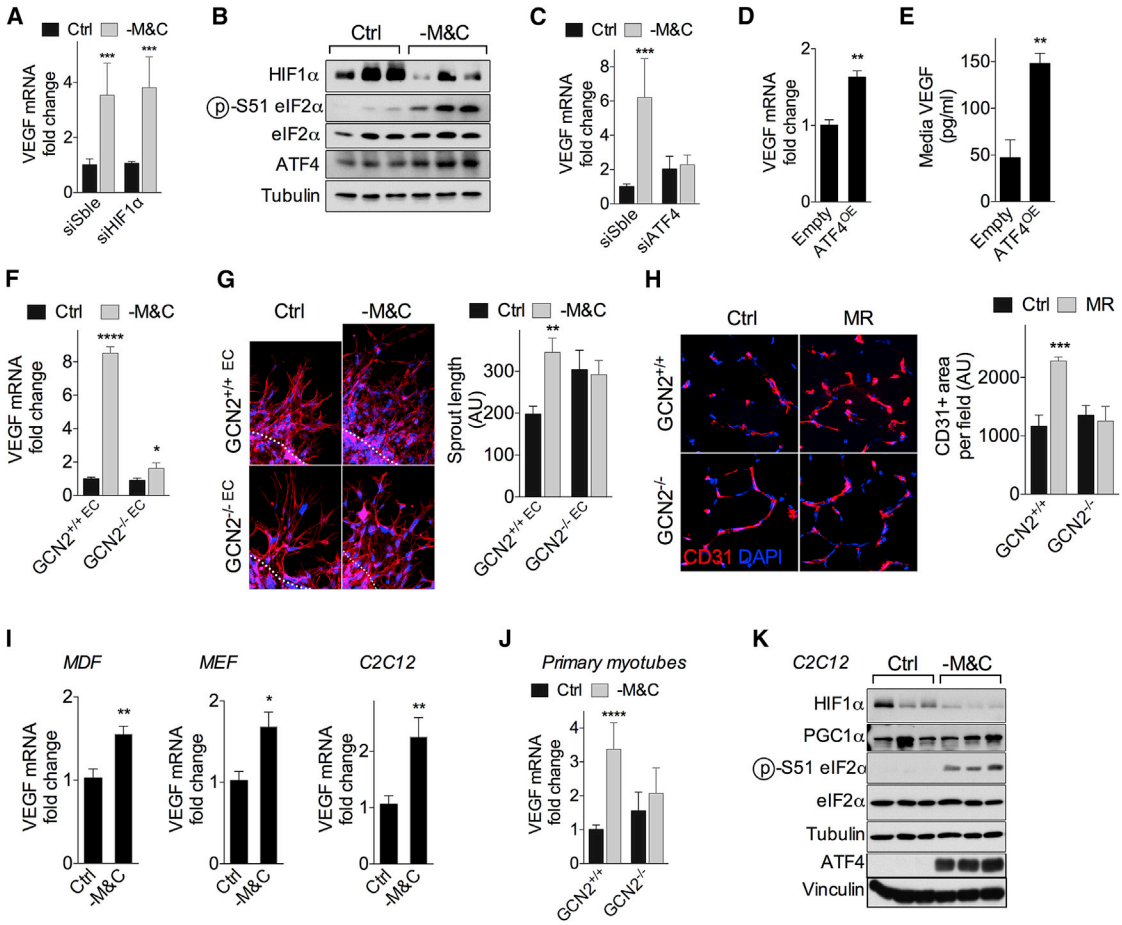

Figure 2. GCN2-Dependent, Hypoxia-Independent Regulation of VEGF and Angiogenesis upon SAA Restriction

(A) Relative VEGF mRNA expression in HUVECs 2 days after transfection with HIF1α siRNA or control scrambled (Sble) siRNA and cultured in control (Ctrl) or SAA-deficient (−M&C) media for 16 hr; n = 5 experiments per group. Error bars indicate SEM.

(B) Immunoblots of HIF1α, eIF2α (p-Ser51, total), and ATF4 in HUVECs cultured as indicated for 16 hr.

(C) Relative VEGF mRNA expression in HUVECs 2 days after transfection with ATF4 or Sble siRNA and cultured as indicated for 16 hr; n = 4 experiments per group. SEM.

(D and E) Relative HUVEC VEGF mRNA expression (D, n = 3 experiments per group; SEM) and secreted VEGF protein concentration in media (E, n = 3–6 experiments per group; SEM) 2 days after transfection with ATF4 overexpression ($ATF4^{OE}$) or control construct (Empty).

(F and G) VEGF mRNA expression (F) and spheroid formation (G) in WT and GCN2KO primary mouse ECs from n = 3 mice per genotype cultured as indicated for 16 hr. For the sprouting assay (G), representative images (left, 40× magnification) and quantification (right) of WT and GCN2KO EC spheroids cultured in the indicated media for 24 hr. Blue, DNA (DAPI); red, F-actin (phalloidin); AU, arbitrary units.

(H) Representative transverse sections (left, 40× magnification) and quantification (right) of CD31-stained gastrocnemius muscle in WT or GCN2KO mice fed for 2–4 weeks on control or MR diet; n = 5–6 mice per group.

(I) VEGF mRNA in MDFs, MEFs, or C2C12 myotubes cultured as indicated for 16 hr; n = 4–6 experiments per group; SEM.

(J) VEGF mRNA expression in WT and GCN2KO primary mouse skeletal myotubes (n = 5 mice per genotype tested at two different passages) cultured as indicated for 16 hr.

(K) Immunoblots of HIF1α, PGC1α, eIF2α (p-Ser51, total), and ATF4 in C2C12 myotubes cultured as indicated for 16 hr.

Error bars indicate SD unless otherwise noted; asterisks indicate the significance of the difference by Student's t test or one-way ANOVA with Sidak's multiple comparisons test between diets *in vivo* or SAA deprivation *in vitro*; *p < 0.05, **p < 0.01, ***p < 0.001. See also Figure S2.

VEGF and Asns transcriptional upregulation upon −M&C (Figures 2C and S2F), while ATF4 overexpression increased VEGF and Asns mRNA expression (Figures 2D and S2G–S2I) and VEGF secretion into the media (Figure 2E) independent of nutrient deprivation.

The requirement for GCN2 was tested in primary ECs isolated from WT (Figure S2J) and GCN2 knockout (GCN2KO) mice. Similar to HUVECs, -M&C significantly increased VEGF and Asns mRNA expression (Figures 2F and S2K) and sprout length (Figure 2G) in WT but not GCN2KO ECs. *In vivo*, GCN2KO mice failed to increase vascular density upon 2–4 weeks of MR compared to controls (Figure 2H).

−M&C also increased VEGF mRNA expression in primary mouse dermal fibroblasts (MDFs), immortalized mouse embryonic fibroblasts (MEFs) and C2C12 myotubes (Figure 2I). In primary skeletal myotubes, VEGF induction upon −M&C required

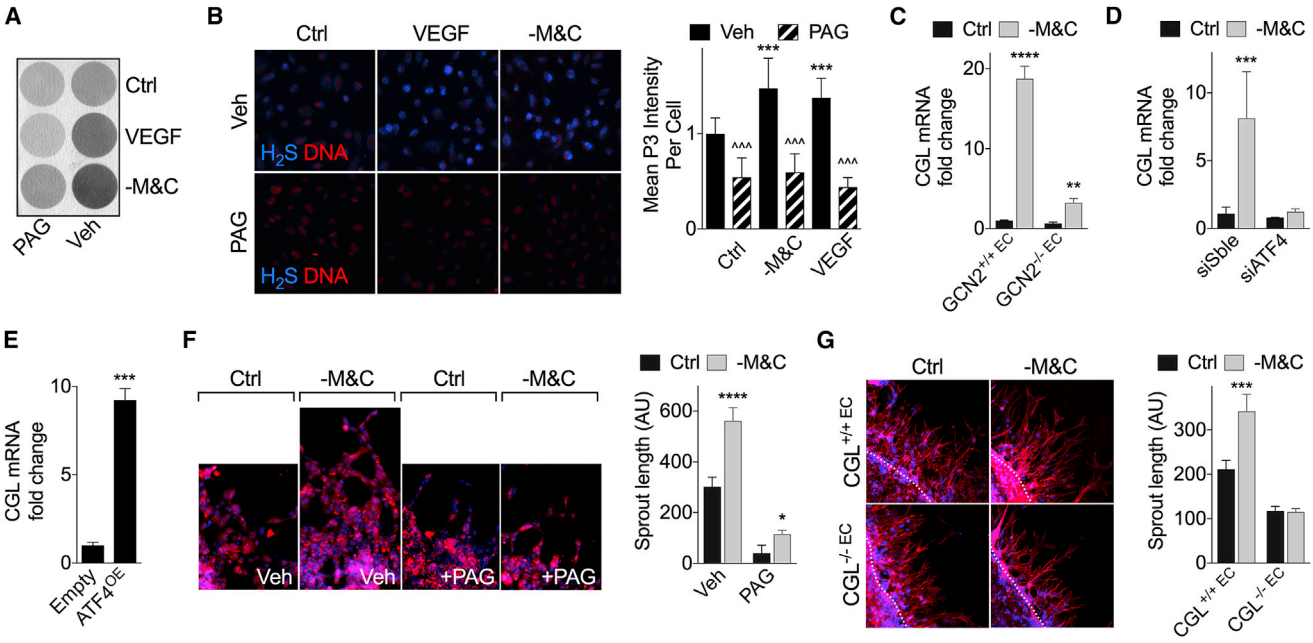

Figure 3. VEGF Signaling and AASR Converge on Endothelial H_2S Production by CGL

(A) Representative H_2S production capacity as indicated by black lead sulfide formation from HUVECs upon VEGF (50 ng/mL) or −M&C treatment in the presence or absence of the CGL inhibitor PAG (100 μM) as indicated for 16 hr.

(B) Representative (left) endogenous H_2S levels (blue, H_2S [P3 fluorescence]; red, DNA [DRAQ5]) and quantification of P3 intensity (right) in HUVECs upon VEGF or −M&C treatment. n = 4 wells per treatment with 4–6 images per well; one-way ANOVA with Sidak's multiple comparisons test versus control (asterisks) or ± PAG within treatment (carets).

(C) CGL mRNA expression in WT and GCN2KO primary mouse ECs cultured from n = 3 mice per genotype in control (Ctrl) or −M&C media for 16 hr.

(D) CGL mRNA expression in HUVECs 2 days after transfection with ATF4 siRNA or control scrambled (Sble) siRNA and cultured in the indicated media for 16 hr. n = 4 experiments per group; SEM.

(E) CGL mRNA Expression in HUVECs 2 days after transfection with ATF4 overexpression or control (empty) plasmid. n = 3 experiments per group; SEM.

(F and G) Representative images (left, 40× magnification) and quantification (right, in triplicate) of spheroids cultured from (F) HUVECs in control or −M&C media for 24 hr in the presence of vehicle (Veh) or PAG and (G) WT or CGLKO primary EC sprouts in control or −M&C media for 24 hr. Blue, DNA (DAPI); red, F-actin (phalloidin); AU, arbitrary units.

Unless otherwise indicated, error bars indicate SD, and asterisks indicate the significance of the difference between diets *in vivo* or SAA levels *in vitro* by Student's t test or one-way ANOVA with Sidak's multiple comparisons test; *p < 0.05, **p < 0.01, ***/p < 0.001. See also Figure S3.

GCN2 (Figure 2J). In MDFs, ATF4 short hairpin RNA (shRNA) prevented the increase in VEGF mRNA by −M&C (Figure S2L). In C2C12 myotubes, VEGF induction coincided with increased eIF2α phosphorylation and ATF4 expression and reduced HIF1α protein levels (Figure 2K). Notably, VEGF induction upon −M&C in C2C12 myotubes was unaffected by HIF1α RNAi KD under normoxic (20%) or hypoxic (<1%) oxygen tensions (Figures S2M–S2O). PGC1α RNAi KD also failed to dampen VEGF induction upon −M&C in C2C12 myotubes (Figure S2P).

Taken together, these data reveal SAA restriction and the GCN2/ATF4-dependent AASR as a novel trigger of increased VEGF expression and angiogenesis independent of hypoxia, HIF1α, or PGC1α.

VEGF Signaling and AASR Converge on Endothelial H_2S Production by CGL

VEGF promotes angiogenesis in part by stimulating CGL-dependent production of the proangiogenic gas H_2S in ECs (Papapetropoulos et al., 2009); however, mechanisms of CGL regulation in ECs and the importance of H_2S in angiogenesis remain poorly understood. H_2S production capacity (Figure 3A) and endogenous H_2S levels (Figure 3B) were similarly increased by −M&C and exogenous VEGF addition and were sensitive to the CGL inhibitor propargylglycine (PAG). −M&C also boosted endogenous H_2S production in primary hepatocytes, while VEGF did not, because hepatocytes lack VEGFR2 (Figure S3A).

CGL is an ATF4 target downstream of the ISR triggered either by ER stress in MEFs (Dickhout et al., 2012) or C deprivation in HepG2 cells (Lee et al., 2008). In primary mouse ECs, CGL mRNA was strongly induced upon −M&C (Figure 3C). This effect was abrogated in ECs lacking GCN2 (Figure 3C) or in HUVECs upon ATF4 KD (Figures 3D and S2F), while ATF4 overexpression increased CGL independent of SAA deprivation (Figure 3E). Importantly, VEGF mRNA was not affected by the absence of CGL (Figure S3B) *in vitro*, consistent with CGL and VEGF as independent downstream targets of the AASR. Interestingly, exogenous VEGF increased CGL mRNA (Figure S3C) and protein (Figure S3D) expression in HUVECs independent of nutrient deprivation, suggestive of a positive feedback loop between

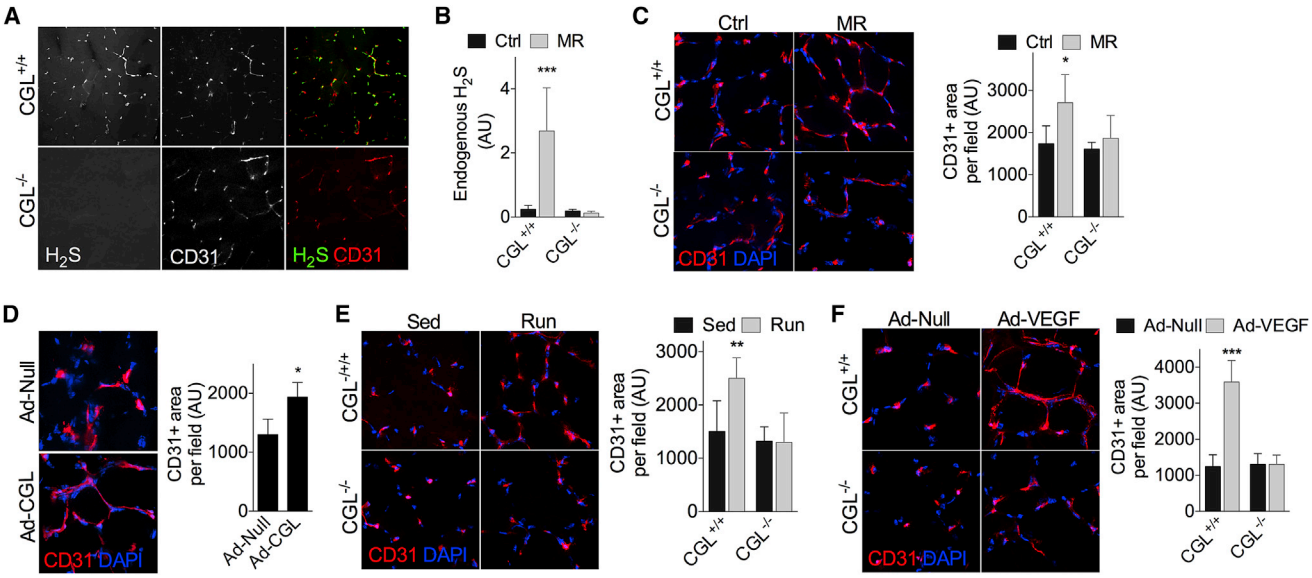

Figure 4. CGL Required for Angiogenesis *In Vivo*

(A) Representative transverse sections (20× magnification) of gastrocnemius muscle from WT and CGLKO mice stained for CD31 and endogenous H_2S.

(B) Quantification of endogenous H_2S in $CD31^+$ ECs in the gastrocnemius muscle of WT and CGLKO mice fed for 2 weeks on control or MR diet as indicated; n = 4–5 mice per group, with quantification of 3–10 images per mouse.

(C) Representative transverse sections (left, 40× magnification) and quantification (right) of CD31-stained gastrocnemius muscle from WT and CGLKO mice fed for 2 weeks on control or MR diet as indicated; n = 4 mice per group.

(D) Representative transverse sections of CD31-stained gastrocnemius muscle (left, 40× magnification) and quantification (right) 2 weeks after Ad-null or Ad-CGL injections. n = 3–4 mice per group; Student's t test.

(E) Representative transverse sections (left, 40× magnification) and quantification (right) of CD31-stained gastrocnemius muscle from WT and CGLKO mice subjected to low-intensity exercise (Run) versus sedentary controls (Sed) for 1 month; n = 4–5 mice per group.

(F) Representative transverse sections of CD31-stained gastroc (left, 40× magnification) and quantification (right) from WT and CGLKO mice 6 days after the final intramuscular injection of control (Ad-null) or $VEGF_{165}$ -expressing (Ad-VEGF) adenovirus; n = 4 mice per group.

Error bars indicate SD; asterisks indicate the significance of the difference between diets or treatments within genotype by one-way ANOVA with Sidak's multiple comparisons test unless otherwise noted; *p < 0.05, **p < 0.01, ***p < 0.001. See also Figure S4.

VEGF and CGL expression, but without affecting expression of the two other H_2S-generating enzymes, CBS or 3-MST.

The functional relevance of endothelial CGL in angiogenic potential *in vitro* was assessed in the EC spheroid assay. Increased sprout length of EC spheroids upon −M&C was prevented by the CGL inhibitor PAG in HUVEC (Figure 3F) and in CGL knockout (CGLKO) mouse ECs (Figure 3G). Thus, CGL is required for angiogenesis induced by −M&C *in vitro*.

CGL Required for Angiogenesis *In Vivo*

We next tested the requirement for CGL-derived H_2S in angiogenesis triggered by MR *in vivo*. Consistent with CGL as the major H_2S producer in EC *in vivo* (Wang, 2012), P3 fluorescence indicative of endogenous H_2S production co-localized with $CD31^+$ cells in fresh-frozen sections of gastrocnemius muscle from WT but not CGLKO mice (Figure 4A). Quantification of P3 intensity in WT and CGLKO mice fed control versus MR diet for 2 weeks confirmed a CGL-dependent increase in EC H_2S production upon MR *in vivo* (Figure 4B). Coincident with failure to increase H_2S, CGLKO mice failed to increase capillary density upon MR *in vivo* relative to WT mice (Figure 4C). Furthermore, the CGL inhibitor PAG partially prevented 40% CR from improving recovery from femoral ligation (Figures S1H and S1I). Taken together, these data are consistent with a requirement for CGL-derived H_2S for angiogenesis triggered by nutrient deprivation.

We next asked if CGL-derived H_2S is sufficient to promote angiogenesis independent of SAA restriction. To this end, we injected CGL-expressing adenovirus into the gastrocnemius muscle of WT mice via intra-muscular injection, likely resulting in CGL overexpression in both myotubes and ECs due to the ability of the Ad5 serotype to infect multiple cell types. Local CGL viral transduction increased muscle H_2S production capacity (Figure S4A) and vascular density (Figure 4D) independent of any other proangiogenic stimulus, suggesting that an increase in CGL-derived H_2S is sufficient to trigger angiogenesis.

To test this apparent general requirement for CGL in angiogenesis independent of the upstream stimulus, we induced angiogenesis by either treadmill exercise training or by VEGF overexpression via intra-muscular injection of VEGF-overexpressing (ad-$VEGF_{165}$) adenovirus. Exercise training increased endogenous VEGF mRNA expression in WT mice (Figure S4B), while both exercise training (Figure 4E) and local VEGF overexpression via adenoviral gene delivery (Figure 4F) increased capillary density in WT but not CGLKO mice. Taken together, these data indicate

that CGL is necessary for VEGF-mediated neovascularization *in vivo* independent of the upstream proangiogenic stimulus.

H_2S Promotes Glucose Uptake and ATP Generation by Glycolysis for EC Migration

Because CGL is a promiscuous enzyme that can convert cystathionine to C as part of the transsulfuration pathway (TSP) but can also use C to produce H_2S and serine, we sought more direct evidence of H_2S as the CGL metabolite relevant to angiogenesis. H_2S addition to standard EC media in the form of NaHS increased proliferation (Figure S5A) and migration across a scratch (Figure 5A). This latter effect was only partially blocked with mitomycinC (MitoC), consistent with migration as a critical factor in H_2S-induced proangiogenic potential. In support of this, HUVECs overexpressing CGL (Ad-CGL) formed lamellipodial projections over larger areas (Figure 5B) coincident with increased migration speed and greater cell body displacement (Figure 5C).

Cell migration requires rapid ATP generation to facilitate actin cytoskeleton rearrangement, which in ECs is met by increasing glycolytic metabolism (De Bock et al., 2013; Schoors et al., 2014). We thus examined glucose uptake and glycolytic ATP production as a function of genetic and pharmacological H_2S modulation. Treatment for 30 min with NaHS increased glucose uptake in HUVECs similar to VEGF (Figure 5D). Interestingly, H_2S-induced glucose uptake was independent of SIRT1 in mouse ECs (Figure S5B).

Glycolytic activity was assessed using several methods. Extracellular acidification rate (ECAR), a surrogate marker of glycolysis, was increased by NaHS treatment in HUVECs (Figure S5C). In primary ECs from WT mice, NaHS and VEGF increased ECAR to a similar level (Figures 5E and S5D), while in CGLKO ECs, ECAR was significantly reduced at baseline and increased by NaHS but not VEGF administration (Figure 5E). Interestingly, accumulation of the end product of aerobic glycolysis, lactate, in the media following NaHS treatment did not reach the level of statistical significance (Figure S5E). We thus measured glycolysis directly using the release of ^3H_2O from C5-^{3}H-glucose and found a significant increase upon NaHS or VEGF treatment (Figure 5F) beginning after 30 min (Figure S5F).

Consistent with increased glycolysis, H_2S boosted intracellular ATP levels over a rapid time course similar to exogenous VEGF (Figure 5G). Both exogenous H_2S addition and CGL overexpression also increased EC migration, and this was sensitive to competitive inhibition of glycolysis by 2-deoxy-D-glucose (2-DG; Figures 5H and 5I). Together, these data support the functional relevance of CGL-derived H_2S in activation of glycolytic ATP generation necessary for proangiogenic migratory behavior.

Steady-state flux analysis was employed to better understand glucose disposal upon NaHS treatment. Addition of ^{13}C1,2-glucose to the media for the final 15 min of a 2-hr NaHS treatment revealed significant changes in labeling of glycolytic intermediates, including an increase in glyceraldehyde-3-phosphate, dihydroxy-acetone-phosphate, and fructose-phosphate (Figure 5J). Interestingly, a significant increase was also observed in the pentose phosphate pathway (PPP) and purine biosynthetic intermediates, including sedoheptulose-7P, phosphoribosyl-1-pyrophosphate, and inosine monophosphate (IMP) (Figure 5J). A significant increase in total unlabelled glycolytic and nucleotide metabolites was also observed (Figure S5G). Increased glucose flux through the PPP is required for angiogenesis (Bierhansl et al., 2017; Vizán et al., 2009) and could also contribute to increased ECAR via CO_2 release during the oxidative phase of the reaction (Figures 5E and S5C) but is not mutually exclusive with the observed increase in glycolytic ATP generation.

Finally, we asked if NaHS and M&C removal triggered similar metabolic responses as predicted if endogenous H_2S production upon −M&C is important for its proangiogenic action. To this end, we performed unbiased metabolomic analyses of HUVECs cultured under standardized media conditions (complete DMEM supplemented with dialyzed fetal bovine syndrome [FBS] and EC growth factors) for 1 hr before addition of NaHS or M&C removal. A comparison of global profiles over a time course following treatment revealed a time-dependent shift upon −M&C away from the control and a striking convergence after 4 hr with the 15-min NaHS profile (Figure 5K). An analysis of all significant changes in the same direction between the 15-min NaHS and −M&C groups included glycolytic and PPP intermediates (Figure 5L).

H_2S Shifts Oxidative/Glycolytic Balance Concomitant with Inhibition of Mitochondrial OXPHOS

By what mechanism does H_2S promote glucose uptake and disposal in ECs? Increased ECAR by NaHS was unaffected by axitinib or the eNOS competitive antagonist L-nitroarginine methyl ester (L-NAME) (Figure S5H). Similarly, NaHS-induced EC migration was unaffected by L-NAME (Figure S5I) or genetic eNOS KD (Figures S5J and S5K), together suggesting a mechanism of action either independent or downstream of proximal VEGFR2 signaling.

In many cell types, inhibition of mitochondrial oxidative phosphorylation (OXPHOS) and transient ATP depletion initiates adaptive responses, including AMP-activated protein kinase (AMPK) activation, that boost glucose uptake and glycolytic ATP production (Hardie et al., 2016). At high concentrations, H_2S can inhibit complex IV of the mitochondrial electron transport chain (ETC) and prevent ATP generation by OXPHOS (Smith et al., 1977); however, whether this mechanism of action contributes to its proangiogenic effect is unknown. Despite the fact that ECs rely predominantly on glycolysis (De Bock et al., 2013), we observed significant changes in glucose flux through the citric acid cycle (reduced citrate/isocitrate and oxaloacetate; Figure 5J), as well as reduced total citrate (Figure S5G), suggesting a block in mitochondrial OXPHOS without an increase in cell death (Figure S5L). Interestingly, labeled and total malate were increased in the same analyses, possibly due to an increase in the cytoplasmic pool, which cannot be distinguished from the mitochondrial pool in whole-cell lysates.

CGLKO ECs displayed increased oxygen consumption rate (OCR) under basal conditions relative to WT cells (Figure 6A), consistent with the ability of endogenous H_2S to inhibit mitochondrial ETC activity. Similarly, exogenous H_2S decreased OCR concomitant with an increase in ECAR to the same levels as the complex V inhibitor oligomycin (Figure 6B). To confirm the predicted effects of H_2S on complex IV activity, OCR was

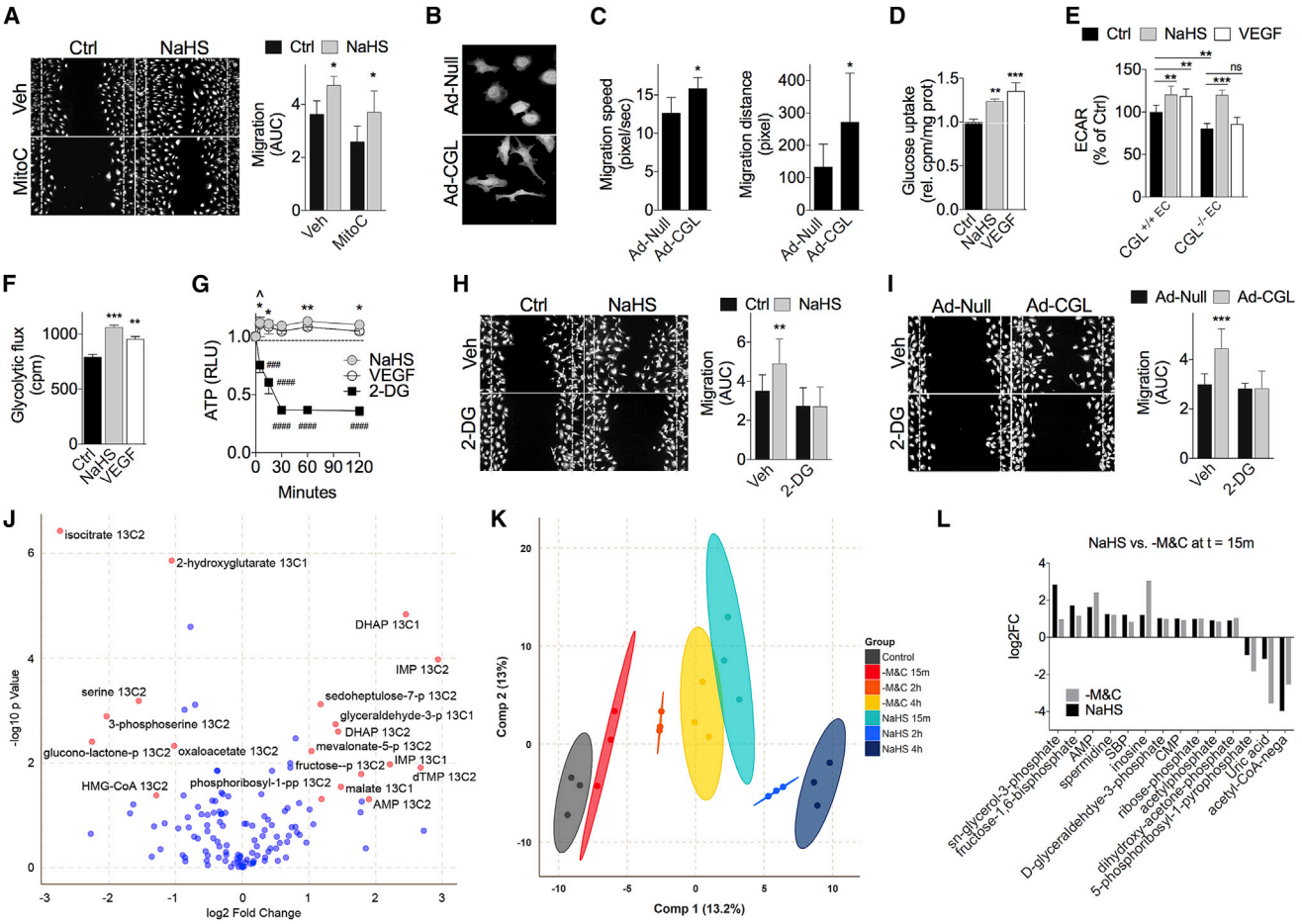

Figure 5. H_2S Promotes Glucose Uptake and ATP Generation by Glycolysis for EC Migration

(A) Representative migration across scratch (left, 10× magnification) and quantification (right) of HUVECs ± 100 μM NaHS in the presence of vehicle or mitomycin C (MitoC, 1 μg/mL) to inhibit proliferation. n = 12 wells each from cells at two different passages; one-way ANOVA with Sidak's multiple comparisons test between control and NaHS within vehicle or MitoC treatment group.

(B and C) Representative images (B) and quantification (C) of migration speed (left, n = 5–7 cells per condition) and distance (right, n = 5–7 cells per condition in x and y directions) from time-lapse video imaging of GFP+ HUVECs infected with control (Ad-null) or CGL adenovirus (Ad-CGL) as indicated; Student's t test.

(D) Relative glucose uptake in HUVECs pretreated with NaHS or 50 ng/mL VEGF for 1 hr. n = 3–6 experiments per group; one-way ANOVA with Dunnett's multiple comparisons test. Error bars indicate SEM.

(E) ECAR in WT and CGLKO primary mouse ECs pretreated for 1 hr with VEGF or NaHS. 10 technical replicates from ECs pooled from six mice per genotype; one-way ANOVA with Sidak's multiple comparisons test as indicated.

(F) Glycolytic flux in HUVECs pretreated for 3 hr with NaHS or VEGF. Representative experiment of six with n = 3 per group; one-way ANOVA with Dunnett's multiple comparisons test.

(G) Time-dependent ATP production in HUVECs pretreated with NaHS or 1 mM 2-DG at t = 0. n = 4 experiments each for NaHS and VEGF and 2 for 2-DG; error bars indicate SEM; two-way ANOVA with Dunnett's multiple comparisons test relative to t = 0 (asterisk, NaHS; caret, VEGF; pound sign, 2-DG).

(H and I) Representative migration (left, 10× magnification) and quantification (right, AUC) of HUVECs treated ± NaHS (H, n = 11 technical replicates per condition) or infected with a control (Ad-null) or CGL adenovirus (Ad-CGL) at a multiplicity of infection of 50 (I, n = 5–6 technical replicates per condition) in the presence of vehicle or 2-DG; one-way ANOVA with Sidak's multiple comparisons test between control and NaHS or Ad-Null and Ad-CGL within 2-DG or vehicle treatment group.

(J) Log2 fold change of C13-labeled metabolites in HUVECs measured by mass spectrometry after 1 hr of NaHS pretreatment compared to control. Red dots, metabolites with false discover rate (FDR) adjusted $p < 0.05$ and absolute value of log2 fold change >1.2; blue dots, metabolites with FDR adjusted $p > 0.05$ and/or absolute value of log2 fold change <1.2.

(K) Plot of the first two components of orthogonal partial least squares discriminant analysis on unlabeled metabolite levels in HUVECs after 15-min, 2-hr, or 4-hr treatment with NaHS or −M&C. Ellipses represent 99% confidence bound for treatment groups.

(L) Average metabolite log2 fold changes after 15 min of NaHS or −M&C. All metabolites that significantly ($p < 0.05$) changed in the same direction in both treatment groups are shown.

Error bars indicate SD unless otherwise indicated; $^{*/\wedge}p < 0.05$, $^{**}p < 0.01$, $^{***/\#\#\#}p < 0.001$, $^{\#\#\#\#}p < 0.0001$. See also Figure S5.

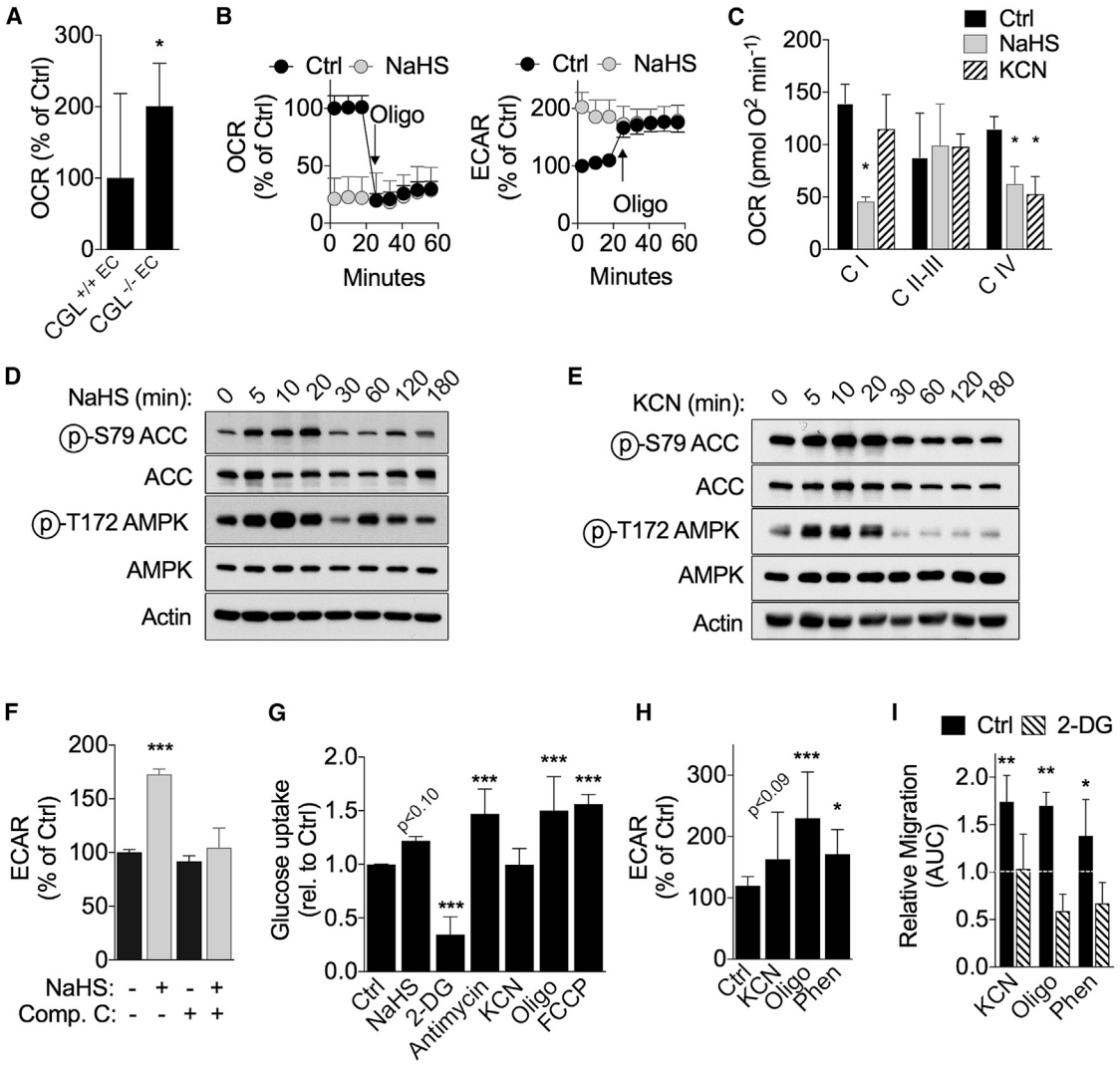

Figure 6. H_2S Shifts Oxidative/Glycolytic Balance Concomitant with Inhibition of Mitochondrial OXPHOS

(A) Basal OCR in WT and CGLKO primary mouse ECs. n = 10 technical replicates from ECs pooled from six mice per genotype; Student's t test.

(B) OCR (left) and ECAR (right) in HUVECs pretreated for 2 hr with 100 μM NaHS followed by oligomycin (oligo, 2.5 μM) injection at the indicated time. Representative experiment with n = 10 technical replicates per treatment.

(C) Mitochondrial complex activity in permeabilized HUVECs pretreated for 1 hr with NaHS or 10 μM KCN; representative experiment with n = 6 technical replicates; one-way ANOVA with Sidak's multiple comparisons test within complex activity group.

(D and E) Immunoblots of acetyl-coenzyme A carboxylase (ACC) (pSer79, total) and AMPK (pThr172, total) in HUVECs treated with NaHS (D) or KCN (E) for the indicated time.

(F) ECAR in HUVECs pretreated for 1 hr with NaHS ± 10 μM compound C (Comp C, an AMPK inhibitor) as indicated. n = 10 technical replicates from ECs pooled from six mice per genotype; one-way ANOVA with Sidak's multiple comparisons test between NaHS treatment within Comp C treatment group.

(G) Relative glucose uptake in HUVECs pretreated with the indicated agent for 1–3 hr. n = 2–8 experiments per group; error bars indicate SEM; one-way ANOVA with Dunnett's multiple comparisons test.

(H) ECAR in HUVECs pretreated for 2 hr with KCN, 2 μM oligo, or phenformin (Phen, 500 μM) expressed as a percent of control over time after addition of 10 mM glucose. n = 12–19 technical replicates; one-way ANOVA with Dunnett's multiple comparisons test.

(I) Migration across scratch expressed as fold change relative to control in HUVECs treated with oligomycin (2 μM), phenformin, or KCN ± 2-DG (1 mM) as indicated. n = 5–12 AUC values per group each from cells at different passages; one-way ANOVA with Sidak's multiple comparisons test versus control without 2-DG treatment.

Error bars indicate SD unless otherwise noted; *p < 0.05, **p < 0.01, ***p < 0.001. See also Figure S6.

measured in isolated HUVEC mitochondria in the presence of NaHS or the complex IV inhibitor potassium cyanide (KCN). In addition to the expected decrease in OCR in the presence of the complex IV substrate TMPD-ascorbate, NaHS also reduced oxygen consumption fueled by pyruvate, consistent with additional ETC inhibition at complex I (Figure 6C).

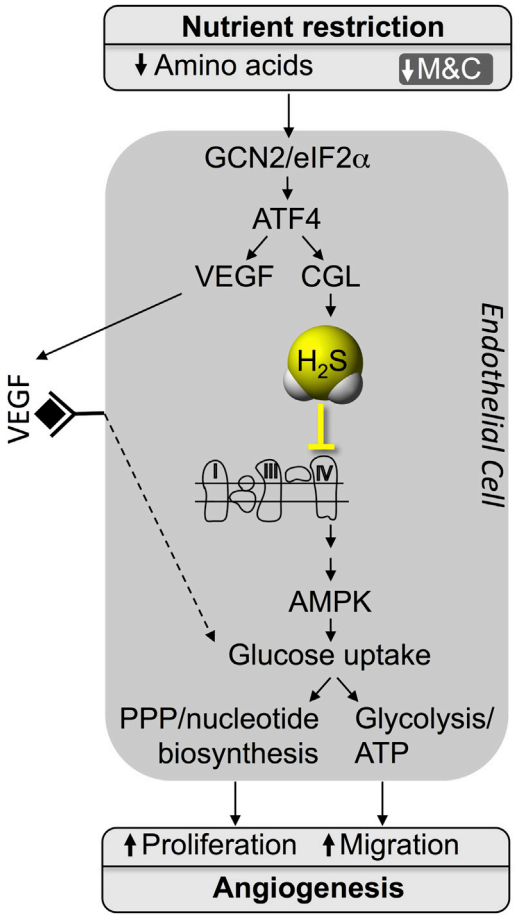

Figure 7. Model for Regulation of Angiogenesis by SAA Restriction
GCN2/ATF4 pathway activation in ECs by SAA restriction induces VEGF expression, as well as CGL-mediated H_2S production, with effects on glucose uptake and utilization via glycolysis and PPP required for EC migration and proliferation.

We next asked if complex IV inhibition was sufficient to trigger AMPK activation in ECs. AMPK was activated within 5 min of NaHS or KCN treatment (Figures 6D and 6E) and returned to baseline after 30 min. Treatment with an AMPK inhibitor (compound C) prevented the increase in ECAR (Figure 6F), glucose uptake, and migration (Figures S6A and S6B). Consistent with the rapid and transient nature of AMPK activation, 10-min NaHS treatment was sufficient to promote EC migration during the subsequent 12-hr period, and this was blocked by compound C (Figures S6C and S6D).

To determine if energy stress was the proximal trigger to AMPK activation, we measured ATP/ADP ratio over a time course following NaHS addition, as well as energy charge 15 min after NaHS addition, but observed no significant changes (Figures S6E and S6F). AMPK can also be activated by upstream kinases, such as CamKKβ (Lee et al., 2012), or reactive oxygen species (ROS) upon hypoxia (Emerling et al., 2009) or nutrient/energy deprivation (Li et al., 2013). However, NaHS-mediated glucose uptake was unaffected by the CamKKβ inhibitor STO-609 (Figure S6G), while mitochondrial ROS failed to increase upon NaHS or KCN treatment (Figure S6H).

Nonetheless, if inhibition of mitochondrial ATP synthesis is the trigger by which H_2S promotes AMPK activation, glycolytic ATP production, and angiogenesis, then any ETC inhibitor could have similar proangiogenic effects. Consistent with this hypothesis, multiple ETC inhibitors targeting different complexes, as well as the uncoupler FCCP, increased glucose uptake (Figure 6G), albeit with slightly different kinetics (Figure S6I). ECAR (Figures 6H and S6J) and glycolytic flux (Figure S6K) were also stimulated by OXPHOS inhibition. Finally, multiple ETC inhibitors stimulated 2-DG-sensitive EC migration (Figures 6I and S6L). Together, these data are consistent with a mechanism of H_2S action in angiogenesis involving transient inhibition of mitochondrial respiration by direct inhibition of ETC, resulting in increased glucose uptake and a shift from OXPHOS to glycolysis and PPP.

DISCUSSION

SAA Restriction as a Proangiogenic Trigger

A model for the proangiogenic pathway activated by SAA restriction and controlled by the GCN2-/ATF4-dependent AASR independent of hypoxia, HIF1α, or PGC1α in ECs is presented in Figure 7. While ATF4 regulation of VEGF expression has been reported in the context of the ISR activated by AA deprivation or ER stress in a human retinal pigmented EC line *in vitro* (Abcouwer et al., 2002) or by mutation of tRNA synthetase genes in zebrafish *in vivo* (Castranova et al., 2016), it has not been previously linked to SAA deprivation via GCN2 in ECs. ATF4 can also activate CGL and H_2S production, which can feed back to increase eIF2α phosphorylation and further activate the ISR (Yadav et al., 2017). Future studies will be required to determine the impact of AA deprivation on other proangiogenic factors, such as fibroblast growth factor (FGF), and if there is any specificity to SAAs. Furthermore, while ATF4 can activate VEGF and CGL expression in multiple different primary cell types *in vitro*, it remains to be determined which cell types *in vivo* are critical for the proangiogenic effects of SAA restriction.

Although H_2S can also be generated by other enzymes, including CBS or 3-MST, we found a genetic requirement for CGL in angiogenesis triggered by nutrient deprivation, exercise, or VEGF injection (Figure 4). CGL is also critical for *de novo* C biogenesis via TSP, linking M cycle metabolites upstream to glutathione and taurine production downstream, perturbation of any of which could potentially contribute to the observed effects. Finally, we acknowledge the apparent paradox of increased endogenous H_2S production in response to restriction of its substrate, C. However, as the source of free C for H_2S generation by CGL is not currently known, it could come from pools distinct from diet-derived or *de novo*-produced C. For example, cytoplasmic glutathione levels that are in the mM range could be utilized as a source of free C, as could products of proteosomal protein degradation or lysosomal autophagy. In support of this latter notion, the increase in H_2S production induced by growth factor (serum) withdrawal in cultured cells is partially abrogated by genetic or pharmacological inhibition of autophagy (Hine et al., 2017), while the benefits of MR on longevity in yeast require autophagy (Ruckenstuhl et al., 2014).

In an accompanying manuscript, Das et al. (2018) report an interaction between H_2S and SIRT1 in the regulation of angiogenesis as evidenced by the ability of H_2S/NMN supplementation in old mice to reverse age-associated loss of muscle vascular density and improved exercise performance. Although the mechanism by which H_2S augments SIRT1 function remains to be elucidated, these data suggest that H_2S and SIRT1 function in a critical axis regulating angiogenesis with the potential to mitigate or reverse oxidative stress-induced and aging-related changes in vascular health using pharmacological agents.

Mechanisms of H_2S Regulation of Energy Metabolism in ECs

H_2S at physiological levels is thought to exert its biological activities through non-mutually exclusive mechanisms, including post-translational modification of target proteins via S-sulfhydration of surface-exposed C residues (Mishanina et al., 2015; Mustafa et al., 2009), direct or indirect antioxidant action (Whiteman et al., 2004; Whiteman et al., 2005), or ATP generation via transfer of electrons to the mitochondrial SQR protein (Goubern et al., 2007; Yong and Searcy, 2001). There is clearly precedent for the potential of H_2S to regulate angiogenesis via S-sulfhydration of target proteins in multiple pathways implicated in angiogenesis, ranging from VEGFR2 signaling (Altaany et al., 2014; Coletta et al., 2012; Tao et al., 2013) to cellular energy metabolism via activation of the rate-limiting glycolytic enzyme GAPDH (Mustafa et al., 2009).

H_2S can also inhibit terminal electron transfer to oxygen (Nicholls and Kim, 1982) at supraphysiological levels, estimated to be greater than 20 μM upon acute treatment of intact human colon carcinoma ECs (Leschelle et al., 2005). Our data are consistent with the potential relevance of this mechanism in regulation of EC oxidative/glycolytic energy balance, although whether levels of endogenously generated H_2S upon SAA deprivation here or in other contexts reach this inhibitory concentration remains unclear (Cooper and Brown, 2008). Consistent with our findings in ECs, an increase in H_2S in pancreatic β cells exposed to ER stress promotes aerobic glycolysis associated with decreased OXPHOS and increased S-sulfhydration of enzymes involved in energy metabolism (Gao et al., 2015). Interestingly, a number of tumors and cancer cells lines also upregulate GCN2 (Lehman et al., 2015; Wang et al., 2013) or H_2S production (Bhattacharyya et al., 2013; Sen et al., 2015; Sonke et al., 2015; Szabo et al., 2013), possibly contributing to the Warburg effect through inhibition of mitochondrial respiration.

STAR★METHODS

Detailed methods are provided in the online version of this paper and include the following:

- KEY RESOURCES TABLE
- CONTACT FOR REAGENT AND RESOURCE SHARING
- EXPERIMENTAL MODEL AND SUBJECT DETAILS
  - Mice
  - Cell Lines and Primary Tissue Culture Studies
- METHOD DETAILS
  - Intramuscular adenoviral-mediated gene delivery
  - Hindlimb ischemia model
  - Laser Doppler perfusion imaging
  - Treadmill exercise training
  - Treadmill exercise test
  - Gene expression analysis by qPCR
  - Immunoblotting
  - VEGF ELISAs
  - Immunohistochemistry and capillary density analysis
  - CD31 FACS analysis
  - H_2S measurements
  - Genetic manipulations in cultured cells
  - Angiogenesis assays in vitro
  - Proliferation
  - Glucose uptake
  - Glycolytic flux analysis
  - ATP and ATP/ADP ratio
  - Energy charge
  - Lactate
  - Cell death and ROS
  - Seahorse
  - Metabolite profiling for glucose flux analyses
  - Global metabolite profiling
- QUANTIFICATION AND STATISTICAL ANALYSIS

SUPPLEMENTAL INFORMATION

Supplemental Information includes six figures and one table and can be found with this article online at https://doi.org/10.1016/j.cell.2018.03.001.

ACKNOWLEDGMENTS

We thank Florent Allagnat for critical discussions and reading the manuscript; Andrew Thompson, Nandan Nurukar, and Rohan Kulkarni for technical assistance; Gokhan Hotamisligil for the use of the Seahorse; John Asara for assistance with metabolomics; Frederick Bowman for the use of the laser Doppler imager; and Constance Cepko for the use of the two-photon microscope. This work was supported by grants from the Swiss National Science Foundation (P1LAP3_158895) to A.L.; the National Science Foundation (NSF-DGE1144152) to L.E.B.; the Canadian Institutes of Health Sciences to R.W.; the NIH (EB00262) to C.S.C.; the American Heart Association (12GRNT9510001 and 12GRNT1207025), the Lea Carpenter du Pont Vascular Surgery Fund, and the Carl and Ruth Shapiro Family Foundation to C.K.O.; and the NIH (AG036712 and DK090629) and the Charoen Pokphand Group to J.R.M.

AUTHOR CONTRIBUTIONS

Conceptualization, A.L., T.M., A.A., M.R.M., A.D., C.H., C.S.C., C.K.O., and J.R.M.; Methodology, A.L., T.M., A.A., M.R.M., J.H.T.-V., C.H., I.B.-S., N.H.K., and L.E.B.; Investigation, A.L., T.M., A.A., M.R.M., A.D., J.H.T.-V., C.H., I.B.-S., N.H.K., L.E.B., J.R., P.M., M.T., and G.S; Resources, R.W., J.-M.C., J.-A.H., K.H.A., C.-H.L., B.D.M., D.A.S., C.S.C., C.K.O., and J.R.M.; Writing, A.L. and J.R.M.; Funding Acquisition, A.L., C.K.O., and J.R.M.

DECLARATION OF INTERESTS

The authors declare no competing interests.

Received: November 2, 2017
Revised: January 17, 2018
Accepted: February 27, 2018
Published: March 22, 2018

REFERENCES

Abcouwer, S.F., Marjon, P.L., Loper, R.K., and Vander Jagt, D.L. (2002). Response of VEGF expression to amino acid deprivation and inducers of endoplasmic reticulum stress. Invest. Ophthalmol. Vis. Sci. *43*, 2791–2798.

Alonso, F., Krattinger, N., Mazzolai, L., Simon, A., Waeber, G., Meda, P., and Haefliger, J.A. (2010). An angiotensin II- and NF-kappaB-dependent mechanism increases connexin 43 in murine arteries targeted by renin-dependent hypertension. Cardiovasc. Res. *87*, 166–176.

Altaany, Z., Ju, Y., Yang, G., and Wang, R. (2014). The coordination of S-sulfhydration, S-nitrosylation, and phosphorylation of endothelial nitric oxide synthase by hydrogen sulfide. Sci. Signal. *7*, ra87.

Arany, Z., Foo, S.Y., Ma, Y., Ruas, J.L., Bommi-Reddy, A., Girnun, G., Cooper, M., Laznik, D., Chinsomboon, J., Rangwala, S.M., et al. (2008). HIF-independent regulation of VEGF and angiogenesis by the transcriptional coactivator PGC-1alpha. Nature *451*, 1008–1012.

Ben-Sahra, I., Howell, J.J., Asara, J.M., and Manning, B.D. (2013). Stimulation of de novo pyrimidine synthesis by growth signaling through mTOR and S6K1. Science *339*, 1323–1328.

Bhattacharyya, S., Saha, S., Giri, K., Lanza, I.R., Nair, K.S., Jennings, N.B., Rodriguez-Aguayo, C., Lopez-Berestein, G., Basal, E., Weaver, A.L., et al. (2013). Cystathionine beta-synthase (CBS) contributes to advanced ovarian cancer progression and drug resistance. PLoS ONE *8*, e79167.

Bierhansl, L., Conradi, L.C., Treps, L., Dewerchin, M., and Carmeliet, P. (2017). Central Role of Metabolism in Endothelial Cell Function and Vascular Disease. Physiology (Bethesda) *32*, 126–140.

Borradaile, N.M., and Pickering, J.G. (2009). Nicotinamide phosphoribosyltransferase imparts human endothelial cells with extended replicative lifespan and enhanced angiogenic capacity in a high glucose environment. Aging Cell *8*, 100–112.

Cai, W.J., Wang, M.J., Moore, P.K., Jin, H.M., Yao, T., and Zhu, Y.C. (2007). The novel proangiogenic effect of hydrogen sulfide is dependent on Akt phosphorylation. Cardiovasc. Res. *76*, 29–40.

Cantó, C., and Auwerx, J. (2009). Caloric restriction, SIRT1 and longevity. Trends Endocrinol. Metab. *20*, 325–331.

Castranova, D., Davis, A.E., Lo, B.D., Miller, M.F., Paukstelis, P.J., Swift, M.R., Pham, V.N., Torres-Vázquez, J., Bell, K., Shaw, K.M., et al. (2016). Aminoacyl-Transfer RNA Synthetase Deficiency Promotes Angiogenesis via the Unfolded Protein Response Pathway. Arterioscler. Thromb. Vasc. Biol. *36*, 655–662.

Coletta, C., Papapetropoulos, A., Erdelyi, K., Olah, G., Módis, K., Panopoulos, P., Asimakopoulou, A., Gerö, D., Sharina, I., Martin, E., and Szabo, C. (2012). Hydrogen sulfide and nitric oxide are mutually dependent in the regulation of angiogenesis and endothelium-dependent vasorelaxation. Proc. Natl. Acad. Sci. USA *109*, 9161–9166.

Colman, R.J., Anderson, R.M., Johnson, S.C., Kastman, E.K., Kosmatka, K.J., Beasley, T.M., Allison, D.B., Cruzen, C., Simmons, H.A., Kemnitz, J.W., and Weindruch, R. (2009). Caloric restriction delays disease onset and mortality in rhesus monkeys. Science *325*, 201–204.

Cooper, C.E., and Brown, G.C. (2008). The inhibition of mitochondrial cytochrome oxidase by the gases carbon monoxide, nitric oxide, hydrogen cyanide and hydrogen sulfide: chemical mechanism and physiological significance. J. Bioenerg. Biomembr. *40*, 533–539.

Das, A., Huang, G.X., Bonkowski, M.S., Longchamp, A., Li, C., Schultz, M.B., Kim, L.-J., Osborne, B., Joshi, S., Lu, Y., et al. (2018). Impairment of an Endothelial NAD^+-H2S Signaling Network Is a Reversible Cause of Vascular Aging. Cell *173*, this issue, 74–89.

De Bock, K., Georgiadou, M., Schoors, S., Kuchnio, A., Wong, B.W., Cantelmo, A.R., Quaegebeur, A., Ghesquière, B., Cauwenberghs, S., Eelen, G., et al. (2013). Role of PFKFB3-driven glycolysis in vessel sprouting. Cell *154*, 651–663.

Dickhout, J.G., Carlisle, R.E., Jerome, D.E., Mohammed-Ali, Z., Jiang, H., Yang, G., Mani, S., Garg, S.K., Banerjee, R., Kaufman, R.J., et al. (2012). Integrated stress response modulates cellular redox state via induction of cystathionine γ-lyase: cross-talk between integrated stress response and thiol metabolism. J. Biol. Chem. *287*, 7603–7614.

Emerling, B.M., Weinberg, F., Snyder, C., Burgess, Z., Mutlu, G.M., Viollet, B., Budinger, G.R., and Chandel, N.S. (2009). Hypoxic activation of AMPK is dependent on mitochondrial ROS but independent of an increase in AMP/ATP ratio. Free Radic. Biol. Med. *46*, 1386–1391.

Fontana, L., Partridge, L., and Longo, V.D. (2010). Extending healthy life span–from yeast to humans. Science *328*, 321–326.

Fukumura, D., Kashiwagi, S., and Jain, R.K. (2006). The role of nitric oxide in tumour progression. Nat. Rev. Cancer *6*, 521–534.

Gao, X.H., Krokowski, D., Guan, B.J., Bederman, I., Majumder, M., Parisien, M., Diatchenko, L., Kabil, O., Willard, B., Banerjee, R., et al. (2015). Quantitative H2S-mediated protein sulfhydration reveals metabolic reprogramming during the integrated stress response. eLife *4*, e10067.

Goubern, M., Andriamihaja, M., Nübel, T., Blachier, F., and Bouillaud, F. (2007). Sulfide, the first inorganic substrate for human cells. FASEB J. *21*, 1699–1706.

Hardie, D.G., Schaffer, B.E., and Brunet, A. (2016). AMPK: An Energy-Sensing Pathway with Multiple Inputs and Outputs. Trends Cell Biol. *26*, 190–201.

Hine, C., Harputlugil, E., Zhang, Y., Ruckenstuhl, C., Lee, B.C., Brace, L., Longchamp, A., Treviño-Villarreal, J.H., Mejia, P., Ozaki, C.K., et al. (2015). Endogenous hydrogen sulfide production is essential for dietary restriction benefits. Cell *160*, 132–144.

Hine, C., Kim, H.J., Zhu, Y., Harputlugil, E., Longchamp, A., Matos, M.S., Ramadoss, P., Bauerle, K., Brace, L., Asara, J.M., et al. (2017). Hypothalamic-Pituitary Axis Regulates Hydrogen Sulfide Production. Cell Metab *25*, 1320–1333.

Hoefer, I.E., van Royen, N., Rectenwald, J.E., Deindl, E., Hua, J., Jost, M., Grundmann, S., Voskuil, M., Ozaki, C.K., Piek, J.J., and Buschmann, I.R. (2004). Arteriogenesis proceeds via ICAM-1/Mac-1- mediated mechanisms. Circ. Res. *94*, 1179–1185.

Katsouda, A., Bibli, S.I., Pyriochou, A., Szabo, C., and Papapetropoulos, A. (2016). Regulation and role of endogenously produced hydrogen sulfide in angiogenesis. Pharmacol. Res. *113* (Pt A), 175–185.

Kilberg, M.S., Pan, Y.X., Chen, H., and Leung-Pineda, V. (2005). Nutritional control of gene expression: how mammalian cells respond to amino acid limitation. Annu. Rev. Nutr. *25*, 59–85.

Kolluru, G.K., Bir, S.C., Yuan, S., Shen, X., Pardue, S., Wang, R., and Kevil, C.G. (2015). Cystathionine γ-lyase regulates arteriogenesis through NO-dependent monocyte recruitment. Cardiovasc. Res. *107*, 590–600.

Kondo, M., Shibata, R., Miura, R., Shimano, M., Kondo, K., Li, P., Ohashi, T., Kihara, S., Maeda, N., Walsh, K., et al. (2009). Caloric restriction stimulates revascularization in response to ischemia via adiponectin-mediated activation of endothelial nitric-oxide synthase. J. Biol. Chem. *284*, 1718–1724.

Lee, J.I., Dominy, J.E., Jr., Sikalidis, A.K., Hirschberger, L.L., Wang, W., and Stipanuk, M.H. (2008). HepG2/C3A cells respond to cysteine deprivation by induction of the amino acid deprivation/integrated stress response pathway. Physiol. Genomics *33*, 218–229.

Lee, H.J., Mariappan, M.M., Feliers, D., Cavaglieri, R.C., Sataranatarajan, K., Abboud, H.E., Choudhury, G.G., and Kasinath, B.S. (2012). Hydrogen sulfide inhibits high glucose-induced matrix protein synthesis by activating AMP-activated protein kinase in renal epithelial cells. J. Biol. Chem. *287*, 4451–4461.

Lehman, S.L., Ryeom, S., and Koumenis, C. (2015). Signaling through alternative Integrated Stress Response pathways compensates for GCN2 loss in a mouse model of soft tissue sarcoma. Sci. Rep. *5*, 11781.

Leschelle, X., Goubern, M., Andriamihaja, M., Blottière, H.M., Couplan, E., Gonzalez-Barroso, M.D., Petit, C., Pagniez, A., Chaumontet, C., Mignotte, B., et al. (2005). Adaptative metabolic response of human colonic epithelial cells to the adverse effects of the luminal compound sulfide. Biochim. Biophys. Acta *1725*, 201–212.

Li, L., Chen, Y., and Gibson, S.B. (2013). Starvation-induced autophagy is regulated by mitochondrial reactive oxygen species leading to AMPK activation. Cell. Signal. *25*, 50–65.

Livak, K.J., and Schmittgen, T.D. (2001). Analysis of relative gene expression data using real-time quantitative PCR and the 2(-Delta Delta C(T)) Method. Methods *25*, 402–408.

Longchamp, A., Alonso, F., Dubuis, C., Allagnat, F., Berard, X., Meda, P., Saucy, F., Corpataux, J.M., Déglise, S., and Haefliger, J.A. (2014). The use of external mesh reinforcement to reduce intimal hyperplasia and preserve the structure of human saphenous veins. Biomaterials *35*, 2588–2599.

Ma, J., and Waxman, D.J. (2008). Modulation of the antitumor activity of metronomic cyclophosphamide by the angiogenesis inhibitor axitinib. Mol. Cancer Ther. *7*, 79–89.

Miller, R.A., Buehner, G., Chang, Y., Harper, J.M., Sigler, R., and Smith-Wheelock, M. (2005). Methionine-deficient diet extends mouse lifespan, slows immune and lens aging, alters glucose, T4, IGF-I and insulin levels, and increases hepatocyte MIF levels and stress resistance. Aging Cell *4*, 119–125.

Mirabella, T., Cilli, M., Carlone, S., Cancedda, R., and Gentili, C. (2011). Amniotic liquid derived stem cells as reservoir of secreted angiogenic factors capable of stimulating neo-arteriogenesis in an ischemic model. Biomaterials *32*, 3689–3699.

Mishanina, T.V., Libiad, M., and Banerjee, R. (2015). Biogenesis of reactive sulfur species for signaling by hydrogen sulfide oxidation pathways. Nat. Chem. Biol. *11*, 457–464.

Mustafa, A.K., Gadalla, M.M., Sen, N., Kim, S., Mu, W., Gazi, S.K., Barrow, R.K., Yang, G., Wang, R., and Snyder, S.H. (2009). H2S signals through protein S-sulfhydration. Sci. Signal. *2*, ra72.

Narkar, V.A., Downes, M., Yu, R.T., Embler, E., Wang, Y.X., Banayo, E., Mihaylova, M.M., Nelson, M.C., Zou, Y., Juguilon, H., et al. (2008). AMPK and PPARdelta agonists are exercise mimetics. Cell *134*, 405–415.

Nicholls, P., and Kim, J.K. (1982). Sulphide as an inhibitor and electron donor for the cytochrome c oxidase system. Can. J. Biochem. *60*, 613–623.

Olsson, A.K., Dimberg, A., Kreuger, J., and Claesson-Welsh, L. (2006). VEGF receptor signalling - in control of vascular function. Nat. Rev. Mol. Cell Biol. *7*, 359–371.

Omodei, D., and Fontana, L. (2011). Calorie restriction and prevention of age-associated chronic disease. FEBS Lett. *585*, 1537–1542.

Orentreich, N., Matias, J.R., DeFelice, A., and Zimmerman, J.A. (1993). Low methionine ingestion by rats extends life span. J. Nutr. *123*, 269–274.

Papapetropoulos, A., Pyriochou, A., Altaany, Z., Yang, G., Marazioti, A., Zhou, Z., Jeschke, M.G., Branski, L.K., Herndon, D.N., Wang, R., and Szabó, C. (2009). Hydrogen sulfide is an endogenous stimulator of angiogenesis. Proc. Natl. Acad. Sci. USA *106*, 21972–21977.

Peng, W., Robertson, L., Gallinetti, J., Mejia, P., Vose, S., Charlip, A., Chu, T., and Mitchell, J.R. (2012). Surgical stress resistance induced by single amino acid deprivation requires Gcn2 in mice. Sci. Transl. Med. *4*, 118ra11.

Potente, M., Urbich, C., Sasaki, K., Hofmann, W.K., Heeschen, C., Aicher, A., Kollipara, R., DePinho, R.A., Zeiher, A.M., and Dimmeler, S. (2005). Involvement of Foxo transcription factors in angiogenesis and postnatal neovascularization. J. Clin. Invest. *115*, 2382–2392.

Potente, M., Ghaeni, L., Baldessari, D., Mostoslavsky, R., Rossig, L., Dequiedt, F., Haendeler, J., Mione, M., Dejana, E., Alt, F.W., et al. (2007). SIRT1 controls endothelial angiogenic functions during vascular growth. Genes Dev. *21*, 2644–2658.

Ruckenstuhl, C., Netzberger, C., Entfellner, I., Carmona-Gutierrez, D., Kickenweiz, T., Stekovic, S., Gleixner, C., Schmid, C., Klug, L., Sorgo, A.G., et al. (2014). Lifespan extension by methionine restriction requires autophagy-dependent vacuolar acidification. PLoS Genet. *10*, e1004347.

Salabei, J.K., Gibb, A.A., and Hill, B.G. (2014). Comprehensive measurement of respiratory activity in permeabilized cells using extracellular flux analysis. Nat. Protoc. *9*, 421–438.

Schoors, S., De Bock, K., Cantelmo, A.R., Georgiadou, M., Ghesquière, B., Cauwenberghs, S., Kuchnio, A., Wong, B.W., Quaegebeur, A., Goveia, J., et al. (2014). Partial and transient reduction of glycolysis by PFKFB3 blockade reduces pathological angiogenesis. Cell Metab. *19*, 37–48.

Sen, S., Kawahara, B., Gupta, D., Tsai, R., Khachatryan, M., Roy-Chowdhuri, S., Bose, S., Yoon, A., Faull, K., Farias-Eisner, R., and Chaudhuri, G. (2015). Role of cystathionine β-synthase in human breast Cancer. Free Radic. Biol. Med. *86*, 228–238.

Singha, S., Kim, D., Moon, H., Wang, T., Kim, K.H., Shin, Y.H., Jung, J., Seo, E., Lee, S.J., and Ahn, K.H. (2015). Toward a selective, sensitive, fast-responsive, and biocompatible two-photon probe for hydrogen sulfide in live cells. Anal. Chem. *87*, 1188–1195.

Smith, L., Kruszyna, H., and Smith, R.P. (1977). The effect of methemoglobin on the inhibition of cytochrome c oxidase by cyanide, sulfide or azide. Biochem. Pharmacol. *26*, 2247–2250.

Sonke, E., Verrydt, M., Postenka, C.O., Pardhan, S., Willie, C.J., Mazzola, C.R., Hammers, M.D., Pluth, M.D., Lobb, I., Power, N.E., et al. (2015). Inhibition of endogenous hydrogen sulfide production in clear-cell renal cell carcinoma cell lines and xenografts restricts their growth, survival and angiogenic potential. Nitric Oxide *49*, 26–39.

Szabó, C. (2007). Hydrogen sulphide and its therapeutic potential. Nat. Rev. Drug Discov. *6*, 917–935.

Szabo, C., Coletta, C., Chao, C., Módis, K., Szczesny, B., Papapetropoulos, A., and Hellmich, M.R. (2013). Tumor-derived hydrogen sulfide, produced by cystathionine-β-synthase, stimulates bioenergetics, cell proliferation, and angiogenesis in colon cancer. Proc. Natl. Acad. Sci. USA *110*, 12474–12479.

Tao, B.B., Liu, S.Y., Zhang, C.C., Fu, W., Cai, W.J., Wang, Y., Shen, Q., Wang, M.J., Chen, Y., Zhang, L.J., et al. (2013). VEGFR2 functions as an H2S-targeting receptor protein kinase with its novel Cys1045-Cys1024 disulfide bond serving as a specific molecular switch for hydrogen sulfide actions in vascular endothelial cells. Antioxid. Redox Signal. *19*, 448–464.

Vizán, P., Sánchez-Tena, S., Alcarraz-Vizán, G., Soler, M., Messeguer, R., Pujol, M.D., Lee, W.N., and Cascante, M. (2009). Characterization of the metabolic changes underlying growth factor angiogenic activation: identification of new potential therapeutic targets. Carcinogenesis *30*, 946–952.

Wang, R. (2012). Physiological implications of hydrogen sulfide: a whiff exploration that blossomed. Physiol. Rev. *92*, 791–896.

Wang, Y. (2014). Molecular Links between Caloric Restriction and Sir2/SIRT1 Activation. Diabetes Metab. J. *38*, 321–329.

Wang, Y., Ning, Y., Alam, G.N., Jankowski, B.M., Dong, Z., Nör, J.E., and Polverini, P.J. (2013). Amino acid deprivation promotes tumor angiogenesis through the GCN2/ATF4 pathway. Neoplasia *15*, 989–997.

Wek, S.A., Zhu, S., and Wek, R.C. (1995). The histidyl-tRNA synthetase-related sequence in the eIF-2 alpha protein kinase GCN2 interacts with tRNA and is required for activation in response to starvation for different amino acids. Mol. Cell. Biol. *15*, 4497–4506.

Whiteman, M., Armstrong, J.S., Chu, S.H., Jia-Ling, S., Wong, B.S., Cheung, N.S., Halliwell, B., and Moore, P.K. (2004). The novel neuromodulator hydrogen sulfide: an endogenous peroxynitrite 'scavenger'? J. Neurochem. *90*, 765–768.

Whiteman, M., Cheung, N.S., Zhu, Y.Z., Chu, S.H., Siau, J.L., Wong, B.S., Armstrong, J.S., and Moore, P.K. (2005). Hydrogen sulphide: a novel inhibitor of hypochlorous acid-mediated oxidative damage in the brain? Biochem. Biophys. Res. Commun. *326*, 794–798.

Yadav, V., Gao, X.H., Willard, B., Hatzoglou, M., Banerjee, R., and Kabil, O. (2017). Hydrogen sulfide modulates eukaryotic translation initiation factor 2α (eIF2α) phosphorylation status in the integrated stress-response pathway. J. Biol. Chem. *292*, 13143–13153.

Yang, G., Wu, L., Jiang, B., Yang, W., Qi, J., Cao, K., Meng, Q., Mustafa, A.K., Mu, W., Zhang, S., et al. (2008). H2S as a physiologic vasorelaxant: hypertension in mice with deletion of cystathionine gamma-lyase. Science *322*, 587–590.

Yong, R., and Searcy, D.G. (2001). Sulfide oxidation coupled to ATP synthesis in chicken liver mitochondria. Comp. Biochem. Physiol. B Biochem. Mol. Biol. *129*, 129–137.

STAR★METHODS

KEY RESOURCES TABLE

REAGENT or RESOURCE	SOURCE	IDENTIFIER
Antibodies		
Anti-pT172-AMPK	Cell Signaling	Cat# 2535
Anti-AMPK	Cell Signaling	Cat# 2532
Anti-ACC1	Cell Signaling	Cat# 4190
Anti-CGL (Anti-Cystathionase)	Abcam	Cat# Ab151769
Anti-CBS	Abcam	Cat# Ab135626
Anti-3MST (Anti-MPST)	Sigma	Cat# HPA001240
Anti-ATF4 (Anti-CREB-2)	Santa Cruz	Cat# Sc-200
Anti-beta Tubulin	Cell Signaling	Cat# 2128
Anti-Actin	Cell Signaling	Cat# 4970
HRP conjugated anti-rabbit	Dako	Cat# P044801-2
Anti-CD31	BD Bioscience	Cat# 557355
Anti-HIF1α	Cayman Chemical	Cat# 10006421
Anti-p-eIF2α Ser51	Cell Signaling	Cat# 9712S
Anti-total eIF2α	Cell Signaling	Cat# 9722S
Anti-Tubulin	Cell Signaling	Cat# 2146S
Anti-CD31-APC	Biolegend	Cat# 102410
Alexa Fluor 555 phalloidin	ThermoFisher	Cat# A34055
Bacterial and Virus Strains		
Ad-CMV-CGL (Ad-mCTH)	Vector Biolabs	Cat# ADV-256305
Ad-CMV-Null	Vector Biolabs	Cat# 1300
Ad-h-VEGFA165	Vector Biolabs	Cat# ADV-227457
Ad-m-ATF4-shRNA	Vector Biolabs	Cat# shADV-253208
Ad-GFP	Vector Biolabs	Cat# 1060
Biological Samples		
Livers (frozen) taken from experimental mouse strains listed in the Experimental Models: Organisms/Strains section	See Experimental Models: Organisms/Strains section	See Experimental Models: Organisms/Strains section
Serum/Plasma (frozen) taken from experimental mouse strains listed in the Experimental Models: Organisms/Strains section	See Experimental Models: Organisms/Strains section	See Experimental Models: Organisms/Strains section
Skeletal muscle (frozen) taken from experimental mouse strains listed in the Experimental Models: Organisms/Strains section	See Experimental Models: Organisms/Strains section	See Experimental Models: Organisms/Strains section
Chemicals, Peptides, and Recombinant Proteins		
NaHS	Sigma	Cat# 161527
GYY4137	Sigma	Cat# SML0100
DL-Propargylglycine	Sigma	Cat# P7888
Passive Lysis Buffer (5x)	Promega	Cat# E1941
PLP (Pyridoxal 5′-phosphate)	Sigma	Cat# P9255
L-cysteine	Sigma	Cat# C7352
Lead (II) acetate trihydrate	Sigma	Cat# 316512
P3 H_2S Detection Probe	From the lab of Prof. K.H. Ahn	Singha et al., 2015
SU5146	Tocris	Cat# 3037

(*Continued on next page*)

Continued

REAGENT or RESOURCE	SOURCE	IDENTIFIER
Ex-527	Cayman Chemical	Cat# 10009798
VECTASHIELD Antifade Mounting Medium with DAPI	Vector laboratories	Cat# H-1200
Potassium Cyanide	Sigma	Cat# 11813
Phenformin	Sigma	Cat# P7045
2-Deoxy-D-Gucose	Sigma	Cat# D8375
Oligomycin A	Sigma	Cat# 75351
FCCP (Carbonyl cyanide 4-(trifluoromethoxy) phenylhydrazone)	Sigma	Cat# C2920
Antimycin A	Sigma	Cat# A8674
MitomycinC	Sigma	Cat# M4287-2MG
Compound C (Dorsomorphin)	Abcam	Cat# Ab120843
Axitinib	Selleckchem	Cat# S1005
L-NAME (hydrochloride)	Cayman Chemical	Cat# 80210
Recombinant human VEGF165	Peprotech	Cat# 100-20
Recombinant murine VEGF165	Peprotech	Cat# 450-32
Propidium Iodine	ThermoFisher Scientific	Cat# P3566
Annexin V	ThermoFisher Scientific	Cat# A13201
Critical Commercial Assays		
Mouse VEGF ELISA	Peprotech	Cat# 900-K99
Mouse VEGF Quantikine ELISA kit	R&D Systems	Cat# MMV00
Human VEGF Quantikine ELISA kit	R&D Systems	Cat# DVE00
Experimental Models: Cell Lines		
Primary mouse endothelial cells prepared from C57BL/6, CGL KO, GCN2 KO and SIRT1 inducible KO mice (freshly isolated in the lab of Dr. James Mitchell or Dr. David Sinclair for each experiment)	Jackson Laboratories and laboratory of Dr. James R. Mitchell	Cat# 000664; this paper; Das et al., 2018
Primary mouse myotubes from GCN2 WT and KO mice	From the laboratory of Dr. James R. Mitchell	This paper
Primary CGL WT and KO mouse tail dermal fibroblasts	From the laboratory of Dr. James R. Mitchell	This paper
Primary mouse hepatocytes from WT mice	From the laboratory of Dr. James R. Mitchell	This paper
Immortalized MEFs	From the laboratory of Dr. James R. Mitchell	This paper
HUVECs	Lonza	Cat# CC-2519
C2C12	ATCC	Cat# CRL-1772
Experimental Models: Organisms/Strains		
C57BL/6 male and female Mice	Jackson Laboratories	Cat# 000664
WT and KO CGL male and female mice on mixed 129/C57BL/6 background	Strain originally from Dr. Rui Wang and bred in the lab of Dr. James R. Mitchell	Yang et al., 2008; Hine et al., 2015
GCN2 WT and KO male and female mice	Strain originally from Dr. David Ron and bred in the lab of Dr. James R. Mitchell	Peng et al., 2012
Oligonucleotides		
si-Scramble (Selective negative control No.1 siRNA)	ThermoFisher Scientific	Cat# 4390843
Mouse si-PGC1a (PPARGC1A)	ThermoFisher Scientific	Cat# n253420

(*Continued on next page*)

Continued

REAGENT or RESOURCE	SOURCE	IDENTIFIER
Mouse si-HIF1a	ThermoFisher Scientific	Cat# s67530
Human si-ATF4	ThermoFisher Scientific	Cat# s1704
Human si-PGC1alpha (PPARGC1A)	ThermoFisher Scientific	Cat# s21394
Human si-HIF1a (HIFA)	ThermoFisher Scientific	Cat# s6539
Human si-eNOS (NOS3)	ThermoFisher Scientific	Cat# s9623
human ACTIN/ACTB F: GTTGTCGACGAC GAGCG R: GCACAGAGCCTCGCCTT	N/A	N/A
human ASNS F: GCGGAGTGCTTCAATGT AAC R: CCAATAAGAAAGTGTTCCTGGG	N/A	N/A
human ATF4 F: CTATACCCAACAGGGCA TCC R: GTCCCTCCAACAACAGCAAG	N/A	N/A
For a full list of all primers used, please see Table S1	N/A	N/A
Recombinant DNA		
prK-ATF4 overexpression plasmid	Addgene	26114
Software and Algorithms		
ImageJ	National Institutes of Health	https://imagej.nih.gov/ij/download.html
GraphPad Prism	GraphPad	Version 7.0
FlowJo	FlowJo	https://www.flowjo.com/solutions/flowjo
Fiji software	GPL v2, Fiji	http://fiji.sc/Fiji
MATLAB R2017A	MathWorks	https://www.mathworks.com/programs/trials/trial_request.html?prodcode=ML

CONTACT FOR REAGENT AND RESOURCE SHARING

Further information and requests for resources and reagents should be directed to and will be fulfilled by the Lead Contact, James R. Mitchell (jmitchel@hsph.harvard.edu)

EXPERIMENTAL MODEL AND SUBJECT DETAILS

Mice

All experiments were performed with the approval of the Harvard Medical Area or Boston University Institutional Animal Care and Use Committee (IACUC). 8-14 week old male or female C57BL/6 mice (The Jackson Laboratory, Bar Harbor, ME) were used for all experiments unless otherwise indicated. Male and female CGL WT and KO mice on a mixed 129/C57BL/6 background (Yang et al., 2008) and GCN2KO and control mice on a C57BL/6 background (Peng et al., 2012) were bred at our facility. Except where indicated, animals were maintained under standard group housing conditions with *ad libitum* (AL) access to food (Purina 5058) and water, 12-hr light/12-hr dark cycles, temperature between 20–23°C with 30%–70% relative humidity.

Experimental diets were based on Research Diets D12450B with approximately 18% of calories from protein (hydrolyzed casein or individual crystalline amino acids (Ajinomoto) in the proportions present in casein), 10% from fat and 72% from carbohydrate. MR diets containing 1.5g methionine (M)/kg food and lacking cysteine (C) (Miller et al., 2005) in the context of a 14% protein/ 76% carbohydrate calorie diet were provided AL. In MR experiments with WT and CGLKO mice, the control diet was supplemented with 4.3g C/kg food to compensate for the inability of CGLKO mice to make C. AL food intake/g body weight was monitored daily for several days and used to calculate calorie restriction (CR) based on initial animal weights. Animals were fed daily with fresh food between 6-7 PM.

Where indicated, axitinib was supplemented at a daily dose of ~30 mg/kg/d in the food as previously described (Alonso et al., 2010; Ma and Waxman, 2008); and PAG was dosed once daily i.p. (10 mg/kg) for the indicated time.

Cell Lines and Primary Tissue Culture Studies

Pooled human umbilical vein endothelial cells (HUVECs) were obtained from Lonza (C2519A, Lonza) and used between passage 1 and 7. HUVECs were cultured in endothelial basal medium (EBM-2) supplemented with 2% FBS and endothelial growth medium SingleQuots (Clonetics, Lonza) at 37°C in a humidified, multigas incubator (Napco Series 8000 WJ, Thermo Scientific) at 5% CO_2 and 3% O_2 achieved by displacing air with nitrogen gas.

Primary mouse endothelial cells were isolated from the lung by collagenase digestion (Liberase, Roche) followed by sequential affinity selection using Dynabeads goat anti-rat conjugated to rat-anti mouse CD31 (BD Biosciences, San Jose, CA), and cultured in endothelial basal medium (EBM-2) supplemented with 2% FBS and endothelial growth medium SingleQuots (Clonetics, Lonza) at 37°C, 5% CO_2 and 3% O_2. At least 3 independent primary mouse EC cultures/genotype was tested per experiment.

Primary mouse hepatocytes were isolated by collagenase digestion, Percoll (GE Healthcare) gradient centrifugation and cultured in William's E media (Sigma) with 5% FBS at 37°C, 5% CO_2 and 3% O_2.

Primary mouse dermal fibroblasts (MDFs) were obtained from tail skin of WT mice following collagenase digestion and cultured in DMEM with 10% FBS at 37°C, 5% CO_2 and 3% O_2.

Primary mouse skeletal myotubes were isolated from leg skeletal muscle following collagenase/dispase digestion and cultured in Ham's F12 with 20% FBS and 10 ng/mL bFGF for approximately one week, then switched to Ham's F12 supplemented with 4% horse serum but lacking bFGF for 7 days at 37°C in 5% CO_2 at normoxia (20% O_2).

C2C12 myoblasts were cultured in DMEM with 10% FBS until they reached 90% confluence, then switched to DMEM supplemented with 4% horse serum for 7 d at 37°C in 5% CO_2 at normoxia (20% O_2).

Immortalized mouse embryonic fibroblasts (MEFs) were cultured in DMEM with 10% FBS at 37°C in 5% CO_2 at normoxia (20% O_2).

The following methionine and cysteine deprivation conditions (-M&C) were used to simulate methionine restriction *in vitro*. For primary EC, when cultures reached confluence, the media was removed and replaced either with complete DMEM ± M&C plus Glutamax (no pyruvate) (Sigma) supplemented with the same amount (2%) of dialyzed FBS and endothelial growth medium SingleQuots (Clonetics, Lonza) for 1 to 24 hr. For hepatocytes, MDFs, primary or C2C12 myotubes and MEF cultures, the media was removed and replaced with complete DMEM ± M&C (plus Glutamax, no pyruvate; Sigma) supplemented with dialyzed FBS (10% for hepatocytes, MDFs and MEFs; 4% for primary skeletal muscle and C2C12 myotubes)

Where indicated, media was supplemented with L-NAME (100 μM), NaHS (100 μM), PAG (100 μM), SU5416 (20 μM), axitinib (10 μM), Ex527 (10 μM), 2-DG (1 mM or 50 mM), Compound C (10 μM) or STO-609 (5 μg/mL). Hypoxia was induced via air displacement with nitrogen gas.

METHOD DETAILS

Intramuscular adenoviral-mediated gene delivery

Local overexpression of CGL or VEGF in gastrocnemius was accomplished by intramuscular injection of 40 μL containing a total of 10^9 PFU of an adenovirus-type 5 (dE1/E3) containing the CMV promoter driving expression of the mouse CGL gene (Ad-mCTH/CGL, GenBank RefSeq BC019483, ADV-256305 Vector Biolabs) or the human VEGF gene (Ad-hVEGFA165 GenBank RefSeq NM_001171626, Vector Biolabs) or the negative control virus Ad-CMV Null (1300 Vector Biolabs) once weekly for 2 weeks.

Hindlimb ischemia model

12 week old C57BL/6 WT mice were anaesthetized with isoflurane and body temperature maintained on a circulating heated water pad. Following a 1 cm groin incision, the neurovascular pedicle was visualized under a microscope (LW Scientific, Z2 Zoom Stereoscope) and the femoral nerve carefully dissected out. The femoral vein (located medially) was separated from the femoral artery (located laterally) allowing electrocoagulation of the left common femoral artery, proximal to the bifurcation of superficial and deep femoral artery while sparing the vein and nerve. Once the artery was occluded, the surgical site was inspected for any residual bleeding (Hoefer et al., 2004; Mirabella et al., 2011).

Laser Doppler perfusion imaging

Laser Doppler perfusion imaging (LDPI) was performed as described previously (Hoefer et al., 2004; Mirabella et al., 2011). Briefly, mice were kept under isoflurane anesthesia, and body temperature maintained on a circulating heated water pad. Blood flow recovery was monitored at d0 (immediately post-surgery), d1, d3, and d10 using an LDPI analyzer (Moor Instruments, DE). The LDPI intensity of the ischemic foot was normalized to the contralateral foot and represented as relative blood flow of the ischemic limb (Ischemic/Non-ischemic ratio). AUCs from I/NI ratios from each animal over time were used for statistical comparisons between groups.

Treadmill exercise training

12 wk old male WT and CGLKO mice were randomized into sedentary or exercise groups. Mice were acclimatized to the treadmill (Columbus Instruments 6 lane treadmill) at 8 m/min for 5 min for 3 d prior to exercise training. Mice ran 30 min/d at 5° incline at 12 m/min for the first wk of training. Mice continued running 30 min/d at 5° incline at 14 m/min for an additional 3 wk to reach 1 mo total of exercise training. Sedentary controls and exercised animals were co-housed. Mice were euthanized 1 hr after the final exercise bout (Narkar et al., 2008).

Treadmill exercise test

2 and 3 days after ischemic injury, mice were acclimatized to the treadmill (Columbus Instruments 6 lane treadmill) at 8 m/min for 5 min prior to exercise testing. At d4, mice were run until exhaustion at 5° incline, 8 m/min for 10 min then 10 m/min for 5 min, with a 2 m/min increase in speed every 5 min (Narkar et al., 2008).

Gene expression analysis by qPCR

Total RNA was isolated from tissues and cells using RNeasy Mini Kit (QIAGEN) and cDNA synthesized by random hexamer priming with the Verso cDNA kit (Thermo). qRT-PCR was performed with SYBR green dye (Lonza) and TaqPro DNA polymerase (Denville). Fold changes were calculated by the $\Delta\Delta C_t$ method (Livak and Schmittgen, 2001) using Hprt, 18S and/or β-Actin genes as standards, and normalized to the experimental control. Human primer sequences are indicated in the Key Resources Table, and mouse primer sequences are additionally found in Table S1.

Immunoblotting

Cells were homogenized with passive lysis buffer (Promega), normalized for protein content, boiled with SDS loading buffer and separated by SDS-PAGE. Proteins were transferred to PVDF membrane (Whatman) and blotted for CGL (ab151769 Abcam), HIF1α (10006421 Cayman Chemical), p-eIF2α Ser51 (9712S Cell Signaling), total eIF2α (9722S Cell Signaling), ATF4 (11815 Cell Signaling), Actin (13E5 Cell Signaling) and Tubulin (2146S Cell Signaling) and secondarily with HRP-conjugated anti-rabbit antibody (Dako).

VEGF ELISAs

Mouse and human VEGF ELISA kits were purchased from Peprotech (900-K99) and R&D System (DEV00), respectively, and assays performed according to manufacturer's instructions on 100 μL of plasma or cell culture media per analysis. For analysis of VEGF protein in muscle, approximately 100 mg of frozen gastrocnemius muscle was pulverized using a mortar and pestle, and the powder transferred to a 1.5 mL microcentrifuge tube containing 150 μL of PBS. The tissue was further disrupted using a mechanical tissue homogenizer (Kimble Kontes Pellet Pestle, Fisher Scientific). After three cycles of freezing and thawing, the tissue suspension was microcentrifuged at max speed for 10 min and the supernatant recovered and stored at −80°C. Lysates were adjusted to 0.5 μg/μL in PBS and assayed using a mouse VEGF ELISA kit from R&D systems (MMV00).

Immunohistochemistry and capillary density analysis

IHC was performed on frozen sections of unfixed gastrocnemius muscle (50 μm for CD31 quantification; 20 μm for CD31/VEGF/IB4 co-staining). After 5 min fixation in PFA 4% and rinsing in PBS, immunostaining was performed as previously described (Longchamp et al., 2014). Primary antibodies included anti-mouse CD31 (BD Bioscience), anti-mouse VEGF (Novus Biologicals) and Isolectin B4 (Life Technologies) at a dilution of 1:100. For capillary density measurements, CD31 area was quantified from randomly photographed 10 μm stack sections (6 images per section, 4 sections per muscle per mouse) using Fiji software (http://fiji.sc/Fiji). All quantifications were performed blindly.

CD31 FACS analysis

Following enzymatic digestion of muscle with collagenase/dispase mix, cells were blocked with mouse FcR blocking reagent (Miltenyl Biotech) and stained for 30 min at 4°C in the dark with CD31APC at 1:100 (BioLegend). Cells were washed and acquired immediately on an LSR II flow cytometer (BD Biosciences) and analyzed with FlowJo. CD31 positive endothelial cells are expressed as a percentage of total cells recovered from the enzymatically digested muscle cells as assessed by forward and side scatter.

H_2S measurements

Detection of H_2S production capacity in live cultures by lead sulfide method

For detection of H_2S production in live cells, growth media was supplemented with 10 mM L-cysteine and 10 μM pyridoxal 5′-phosphate hydrate (PLP, Sigma), and a 6x4 inch piece of lead acetate paper, made by soaking 703 size blotting paper (VWR) in 20 mM lead acetate (Sigma) and then vacuum dried, was placed over the plate for 2-24 hr of further incubation in a CO_2 incubator at 37°C until lead sulfide was detected but not saturated.

Detection of endogenous H_2S with fluorescent P3 probe in cultured cells or frozen tissue sections

For detection of endogenous H_2S production in live adherent cells, growth media was supplemented with 10 μM P3 probe (Singha et al., 2015) for 30 min prior to fixation. Quantification was performed by calculating the average P3 signal intensity per cell. Cell areas were automatically segmented using brightfield images. Values presented are average P3 intensity per cell, corrected for total cell area. Analyses were performed using MATLAB R2017A.

For detection of endogenous H_2S production in tissue sections, 50 μm frozen sections of unfixed gastrocnemius muscle were incubated with 20 μM P3 probe for 5 min and washed 2X with PBS. Sections were then fixed for 5 min in 4% PFA prior to immunostaining using a 2 photon microscope (Zeiss LSM780 w/ Mai Tai HP 2-photon laser (Spectra Physics) at 880 nm excitation and 520-550 nm emission (Singha et al., 2015).

Genetic manipulations in cultured cells

siRNA knockdown

siRNA knockdown of human activating transcription factor 4 (ATF4), human endothelial nitric oxide synthase (eNOS), human hypoxia-inducible factor 1α (HIF1α), PGC1α (PPARGC1A) in HUVECs as well as mouse HIF1α and PGC1α in C2C12 myoblasts was performed using lipofectamine RNAiMAX (Life Technologies) and 30 nM siRNA purchased from Ambion (Ambion, ThermoFisher) as

described previously (Hine et al., 2015). All experiments were performed 2 days after transfection. Knockdown was confirmed by immunoblot and/or qPCR.

shRNA knockdown of ATF4

MDFs were infected overnight in complete medium and collected 2 days later using Ad-m-ATF4-shRNA or the negative control virus Ad-CMV Null adenovirus amplified and purified by Vector Biolabs (Philadelphia, PA, U.S.A.).

ATF4 overexpression

ATF4 overexpression in HUVECs was performed using Lipofectamine 2000 (Life Technologies) and 1 μg of prK-ATF4 plasmid per well (12-well format) overnight. All experiments were performed 2 days after transfection. Overexpression was confirmed by immunoblot and/or qPCR.

Adenoviral-mediated CGL overexpression

HUVECs were infected overnight in complete medium using Ad-m-CTH or the negative control virus Ad-CMV Null adenovirus amplified and purified by Vector Biolabs (Philadelphia, PA, U.S.A.) and collected 2 days later.

Angiogenesis assays in vitro

Migration assay

ECs were seeded at 100,000 cells per well in a 24-well plate in EGM with 2% serum and growth factors (Lonza). ~12 hr later, media was switched to EGM without serum/growth factors, and in some cases mitotically arrested (1 μg/mL MitoC). A single scratch was created using a sterile p200 pipette tip on a confluent field of EC. Floating cells were washed away and EGM (or DMEM ± M&C media) with dialyzed serum and growth factors replaced, including treatments. Repopulation/migration across the scratch was recorded by phase-contrast microscopy every 4 hr for up to 20 hr using a digital camera. Migration across the scratch (gap area at t = X hr relative to t = 0 hr) was determined at each time point from digital images using ImageJ software.

Tube formation

Formation of tube networks was assessed as described previously (Borradaile and Pickering, 2009). HUVECs were seeded at 10,000 cells per well in a 24-well plate (Corning) coated with 150 μL Cultrex reduced growth factor basement membrane extract (Trevigen). Following an 18 hr-incubation, resulting tube networks were analyzed by light microscopy (Nikon Eclipse TiE). The total length of tubule networks and the number of branch points were quantified by ImageJ software.

Spheroid capillary sprouting assay

Hanging drops of HUVECs or primary mouse ECs in EGM2 (De Bock et al., 2013) were embedded in Matrigel® (Corning) and cultured in the indicated media for 24 hr to induce sprouting. Compounds were added at the indicated concentrations during the gel culture step, using corresponding vehicle concentrations as control. Spheroid cultures were stained with phalloidin diluted 1:500 in PBST for 1 hr at RT and counterstained with DAPI. Images were captured with a Zeiss LSM 510 Meta NLO confocal microscope (oil objectives: x 40 with NA 1.3, x 63 with NA1.4, x 100 with NA 1.3; Carl Zeiss, Munich, Germany) or a Leica laser-scanning SP5 confocal microscope (Leica, Manheim, Germany). Analysis of the sprout length was performed using ImageJ software.

Proliferation

HUVECs were cultured to 60% confluency in a 12-well plate on glass coverslips, washed with PBS and incubated for 24 hr in EGM2 containing 0.1 mM BrdU. Immunostaining was performed on cells washed and fixed for 5 min in −20°C acetone, air-dried, rinsed in PBS and permeabilized for 1 hr in PBS supplemented with 2% BSA and 0.1% Triton X-100. BrdU positive nuclei were automatically detected using the ImageJ software and normalized to the total number of DAPI-positive nuclei.

Glucose uptake

For VEGF and NaHS treatment ± Compound C (10 μM) (Figures 5D and S6A), HUVECs were pretreated for 1 hr with 50 ng/ml VEGF (Peprotech) or 100 μM NaHS. Cells were then depleted in Krebs-Ringer Bicarbonate Buffer (KRB; NaH_2PO_4/Na_2HPO_4 10 mM, NaCl 136 mM, KCl 4.7 mM, MgSO4 1.25mM, CaCl2 1.25mM, pH7.4), without glucose and serum for 30 min and then incubated for 6 min in a solution containing 0.5 μCi ^{3}H-2-DG. On ice, cells were then washed in cold PBS 3 times, lysed, and sample counted in a liquid scintillation counter. Samples were normalized to protein content as measured from the same cells by BCA. For remaining glucose uptake experiments (Figures S5B, S6G, S6I and 6G), EC were treated with NaHS (100 μM), KCN (10 μM), Antimycin A (2.5 μM), Oligomycin (2 μM), or FCCP (1.5 μM) for 45, 75 or 195 min in EGM-2. When indicated, inhibitors were added 30 min before the addition of the tracer. Fifteen min before the termination of the experiment, 0.4 μCi of ^{3}H-2-DG was added to each well (1 mL final volume, 12-well format). At the end of the incubation the plate was rapidly transferred on ice, media removed and washed 4 times with PBS + BSA 0.1%. Finally, cell lysis was performed with NaOH 0.2% + SDS 0.5%. Lysate (500 μL) was mixed with scintillation fluid (5 mL) and sample radioactivity measured in a scintillation counter (Beckman).

Glycolytic flux analysis

HUVECs were cultured with standard media (EGM-2), and stimulated for up to 3 hr with test compounds (NaHS 100 μM, VEGF 50ng/mL, Antimycin A 2.5 μM, Oligomycin 2 μM, or 2-DG 1mM). 15 min before the end of the incubation, 5 μCi D-[5-3H(N)]-glucose was added to 1.5 mL media (12-well format), then the plate was rapidly transferred on ice, and the media (1.5 mL) transferred into a 5 mL vial. One PBS wash (1.5 mL) was performed and liquid combined with media. The vial was inserted into a 50 mL tube pre-filled

with 3 mL water. The tube was tightly capped and evaporation was performed at room temperature for 48 hr. Finally, 2 mL of water was collected from the 50mL tube and mixed with 10 mL of scintillation fluid. Sample radioactivity was measured in a scintillation counter (Beckman).

ATP and ATP/ADP ratio

Cells in a 96-well format were treated with NaHS, VEGF or 2-DG in a reverse time course. ATP was measured by addition of 70 μL of Cell TITER-Glo (Promega), plate incubated in the dark for 10 min and luminescence quantified by a plate reader (BioTek instruments). ADP/ATP ratio was calculated after measuring ADP and ATP by a commercially available enzymatic assay (ApoSENSOR, BioVision), according to the manufacturer's instructions.

Energy charge

Steady-state mass spec measurements of AMP, ADP and ATP were used to calculate energy charge using the following equation: (ATP +1/2ADP)/(ATP + ADP + AMP).

Lactate

Lactate in HUVEC culture media was measured after 1.5-6 hr of treatment with NaHS (100 μM). The assay was performed using a plate-based colorimetric assay (Cell Biolabs) according to the manufacturer's protocol.

Cell death and ROS

Apoptosis and cell death were measured after 12 hr treatment with NaHS (100 μM) or –M&C using a FACS-based annexin V/propidium iodide assay according to the manufacturer's protocol (BD Biosciences).

Reactive oxygen species were measured after 15 min, 1 hr and 2 hr incubations with NaHS (100 μM), FCCP (2 μM) or KCN (10 μM). Menadione (10 μM) was used as a positive control. Cells were stained for 15 min with CellROX Green dye in the treatment media, fixed with 2% paraformaldehyde and measured using FACS.

Seahorse

Cellular oxygen consumption and extracellular acidification rate was measured using the Seahorse Cell Metabolism Analyzer XF96 (Seahorse Biosciences). Cells were plated at a density of 12,000 cells and untreated or pretreated with 100 μM NaHS, 10 μM KCN or 500 μM phenformin for 2 hr. After 2 hr, media was changed to unbuffered XF assay media with 0 or 11 mM glucose, 0 or 2 mM glutamine and pyruvate at pH7.4 and basal OCR and ECAR measured for 5 blocks of 2 min mixing and 5 min measuring. Glucose (10 mM final), 2-DG (50 mM final) and Oligomycin (2.5 μM final) were injected at indicated times. All plates were normalized to protein content as measured from the same cells after Seahorse by BCA.

Mitochondrial respiration in permeabilized cells using complex-specific substrates was measured in a Seahorse Cell Metabolism Analyzer XF24 (Seahorse Biosciences) as previously described (Salabei et al., 2014). Briefly, cells were plated at a density of 100,000 cells in EGM-2. Four hr later, cells were pretreated with 100 μM NaHS or 10 μM KCN for 1 hr, then washed with MAS buffer and incubated with MAS buffer containing 10 mM pryruvate, 2 mM malate, 4 μM FCCP and 25 μg/mL Saponin for 1 hr. OCR was measured for 10 blocks of 1 min mixing and 2 min measuring. Rotenone (1 μM final), Succinate (10 mM final), Antimycin A (20 μM final), and TMPD/Ascorbate (0.5 mM/2 mM final) were injected in order.

Metabolite profiling for glucose flux analyses

To determine the relative levels of intracellular metabolites, extracts were prepared and analyzed by LC/MS/MS. Triplicate 15-cm confluent plates were incubated in EGM-2 media in presence or absence of 100 μM NaHS 105 min prior to extraction. For D-[1,2-^{13}C]- glucose flux studies, cells were washed once with serum- and glucose free DMEM and then incubated in DMEM containing a 10 mM 1:1 mixture of D-[1,2-^{13}C]-glucose and unlabeled D-glucose for 15 min. Metabolites were extracted on dry ice with 4 mL 80% methanol (−80°C) as described previously (Ben-Sahra et al., 2013). Insoluble material was pelleted by centrifugation at 3000*g* for 5 min, followed by two subsequent extractions of the insoluble pellet with 0.5 mL 80% methanol, with centrifugation at 16,000*g* for 5 min. The 5 mL metabolite extract from the pooled supernatants was dried down under nitrogen gas using an N-EVAP (Organomation Associates).

Dried pellets were resuspended using 20 μL HPLC grade water for mass spectrometry. 10 μL was injected and analyzed using a 5500 QTRAP triple quadrupole mass spectrometer (AB/SCIEX) coupled to a Prominence UFLC HPLC system (Shimadzu) via selected reaction monitoring (SRM). Some metabolites were targeted in both positive and negative ion mode for a total of 287 SRM transitions using pos/neg polarity switching. ESI voltage was +4900V in positive ion mode and –4500V in negative ion mode. The dwell time was 3 ms per SRM transition and the total cycle time was 1.55 s. Approximately 10-14 data points were acquired per detected metabolite. Samples were delivered to the MS via normal phase chromatography using a 4.6 mm i.d. x 10 cm Amide Xbridge HILIC column (Waters) at 350 μL/min. Gradients were run starting from 85% buffer B (HPLC grade acetonitrile) to 42% B from 0-5 min; 42% B to 0% B from 5-16 min; 0% B was held from 16-24 min; 0% B to 85% B from 24-25 min; 85% B was held for 7 min to re-equilibrate the column. Buffer A was comprised of 20 mM ammonium hydroxide/20 mM ammonium acetate (pH = 9.0) in 95:5 water:acetonitrile. Peak areas from the total ion current for each metabolite SRM transition were integrated using

MultiQuant v2.0 software (AB/SCIEX). For stable isotope labeling experiments, custom SRMs were created for expected ^{13}C incorporation in various forms for targeted LC/MS/MS. Samples were quantile normalized and log transformed and metabolites were pareto scaled prior to analysis. Analyses were performed using R version 3.3.2.

Global metabolite profiling

HUVECs grown in EBM-2 media with BulletKit were switched to DMEM with 2% dialyzed FBS and all non-serum BulletKit components. After a 1 hr equilibration period, cells were switched to treatment media (control, -M&C, NaHS 100 μM). After the treatment period (15 min, 2 hr, 4 hr) cells were collected and analyzed for total metabolite profile by mass spectrometry using the methods detailed in the preceding section.

QUANTIFICATION AND STATISTICAL ANALYSIS

Data are displayed as means ± standard deviation (SD) and statistical significance assessed in GraphPad Prism using Student's t test, one-way or two-way ANOVA unless otherwise specified. A P value of 0.05 or less was deemed statistically significant.

Cell

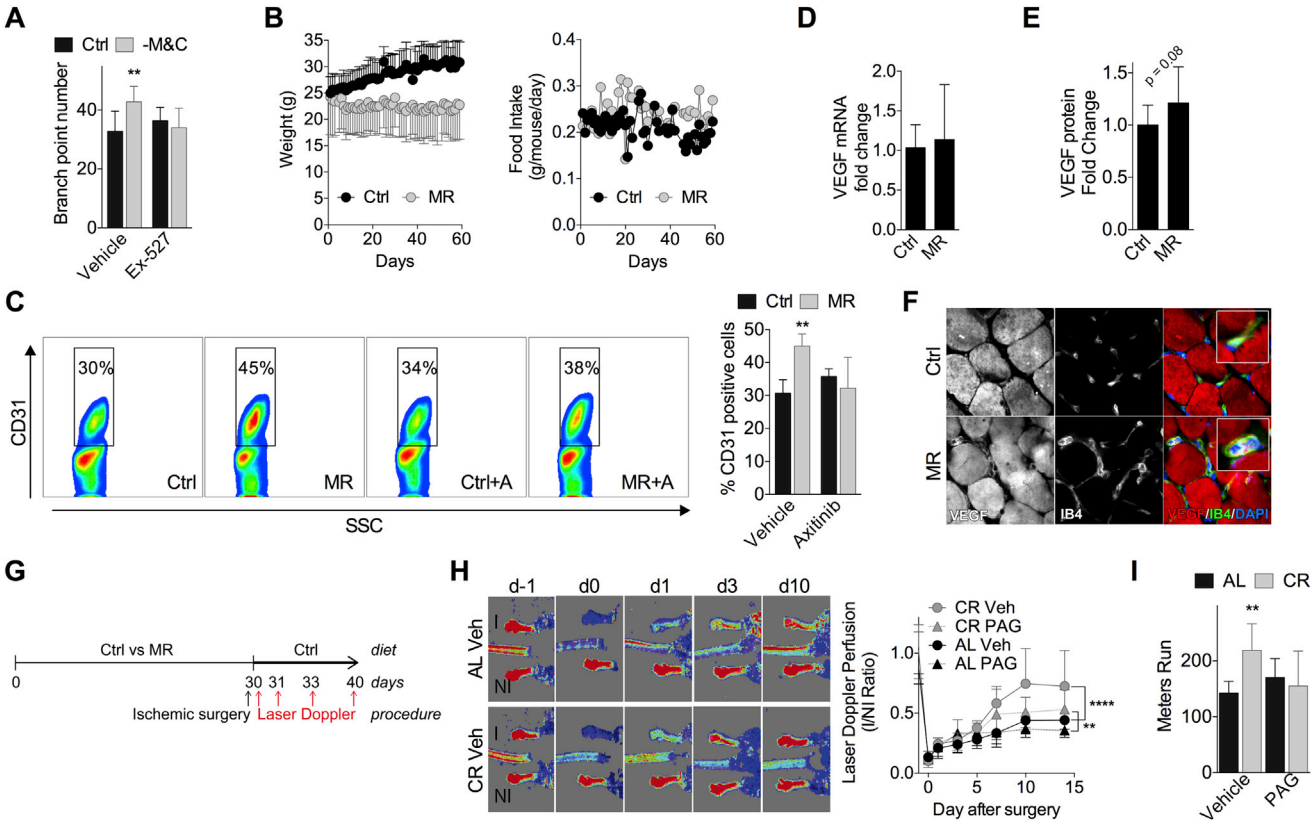

Figure S1. SAA Restriction Induces Endothelial VEGF Expression *In Vitro* and Functional Angiogenesis *In Vivo*, Related to Figure 1

(A) Tube formation assay: Quantification of tube branch points per field of view in HUVECs seeded onto growth factor-replete Matrigel and incubated in the indicated media ± SIRT1 inhibitor Ex-527 for 18 hr; n = 8-10 data points/condition.

(B) Daily body weight (left, n = 5 mice/group) and food intake expressed as grams of food eaten per gram of mouse body weight (right, n = 2 cages/group) of mice given *ad libitum* access to M restricted (MR) versus control (Ctrl) diet for 2 mo in a representative experiment.

(C) Representative flow cytometric analysis of CD31 positive cells from gastrocnemius muscle of mice fed for 2 wk on Ctrl or MR diets with or without VEGFR2 inhibition (axitinib, +A) expressed as a percentage of total cells recovered from the enzymatically digested muscle tissue; quantification at right (n = 3-6 mice/group).

(D) Expression of VEGF mRNA in gastrocnemius muscle of mice subject to MR for 2-8 wk expressed relative to Ctrl diet group; n = 22-23/mice group.

(E) VEGF protein levels in extracts of muscle from mice on the indicated diet for at least 2 wk as determined by ELISA; n = 11-13/group.

(F) Representative transverse sections of gastrocnemius muscle stained for VEGF (left, 40X mag), IsolectinB4 (IB4, middle, 40X mag) and merged (VEGF red, IB4 green, DAPI blue; right, insert 160X mag) in mice preconditioned for 2 mo on control (Ctrl) or M restricted (MR) diets.

(G) Schematic representation of the hindlimb ischemia procedure.

(H and I) Longitudinal Doppler imaging of blood flow (H) and distance run on treadmill exercise test (I) following ischemia in WT mice preconditioned on a complete diet fed *ad libitum* (AL) or calorie restricted daily by 40% of the AL amount (CR) for 1 mo prior to femoral artery ligation, +/−propargylglycine (PAG) daily for 1 wk prior to ligation and 2 wk after as indicated. (H) Left: representative infrared images on the indicated after ligation (I, ischemic; NI, non-ischemic). Right: quantification of blood flow recovery with individual animal AUCs used for statistical comparisons; n = 6 mice/group. (I) Distance run on treadmill exercise test on d4 after ligation of the indicated groups from (H).

Error bars indicate SD; asterisks indicate the significance of the difference by Student's t test or one-way ANOVA with Sidak's multiple comparisons test between diets *in vivo* or sulfur amino acid levels *in vitro*; *p < 0.05, **p < 0.01, ***p < 0.001, ****p < 0.0001.

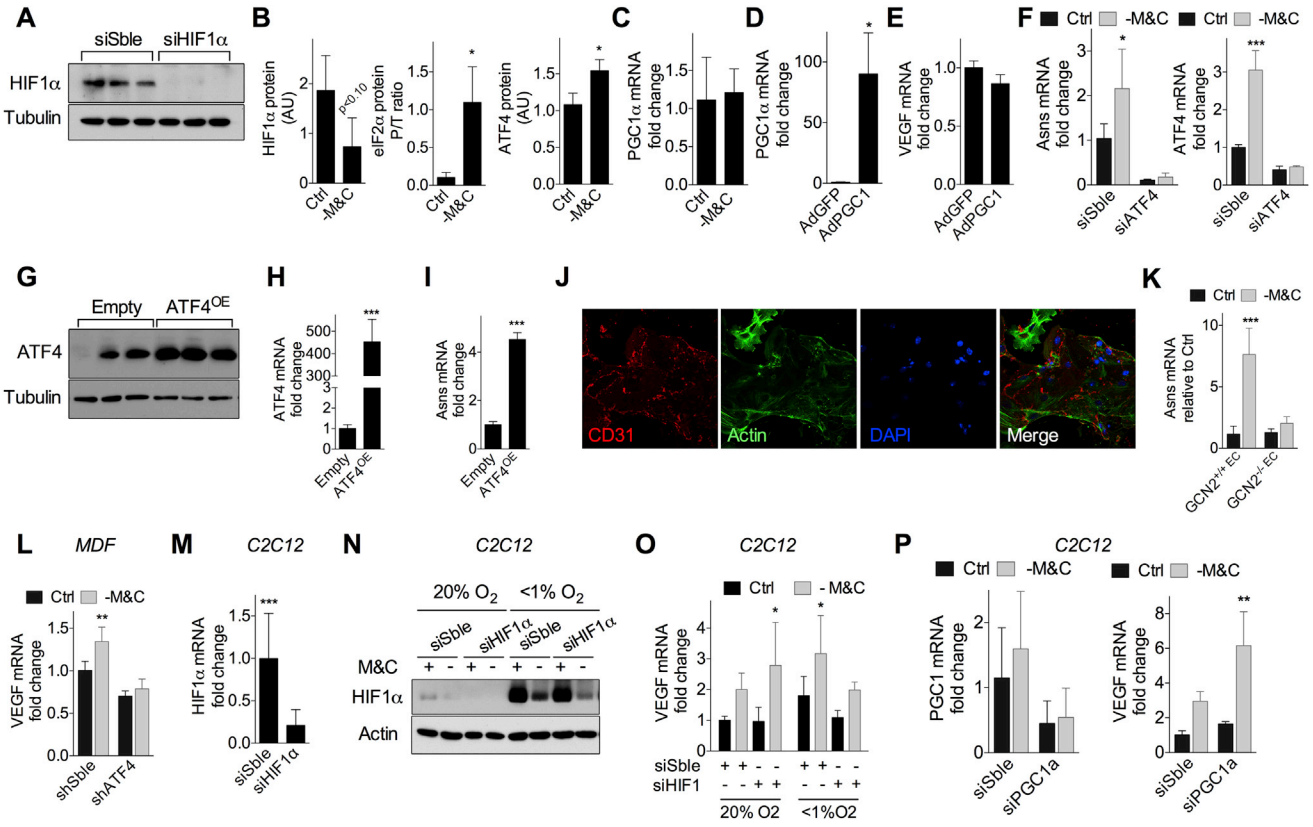

Figure S2. GCN2-Dependent, Hypoxia-Independent Regulation of VEGF and Angiogenesis upon SAA Restriction, Related to Figure 2

(A) Immunoblot of HIF1α protein in HUVECs 2 d after transfection with HIF1α siRNA or control scrambled (Sble) siRNA.

(B) Quantification of immunoblots from Figure 2B of the indicated protein from HUVEC extracts after culturing in control (Ctrl) or M&C deficient media (−M&C).

(C) PGC1α mRNA levels of HUVECs cultured in the indicated media for 16 hr; n = 4 experiments/group, error bars indicate SEM.

(D and E) PGC1α (D) and VEGF (E) mRNA levels in HUVECs 2 d after transfection with a PGC1α overexpressing construct, and expressed relative to cells transfected with a control AdGFP vector; n = 3 experiments/group, SEM.

(F) Asns (left) and ATF4 (right) mRNA expression in HUVECs 2 d after transfection with ATF4 siRNA or control scrambled (Sble) siRNA and cultured in the indicated media for 16 hr; n = 4 experiments/group, SEM.

(G–I) Immunoblot of ATF4 protein (G), mRNA expression of ATF4 (H) and Asns (I) in HUVECs 2 d after transfection with a CMV-driven ATF4 overexpressing construct ($ATF4^{OE}$) or empty vector (Empty).

(J) Representative images of primary WT mouse ECs stained for CD31 (red), Actin (green) and DAPI (blue) at 40X mag; n = 3 experiments/group, SEM.

(K) Asns mRNA in WT and GCN2KO primary mouse ECs from n = 5-6 mice per genotype cultured as indicated for 16 hr.

(L) VEGF mRNA in MDFs 2 d after infection with shATF4 or control scrambled adenovirus and cultured for the final 16 hr as indicated; n = 5-8 experiments/group, SEM.

(M) HIF1α mRNA expression in C2C12 cells 2 d after transfection with HIF1α siRNA or control scrambled (Sble) siRNA and then cultured for an additional 16 hr in control media; n = 11-12 experiments/group, SEM.

(N and O) C2C12 HIF1α protein level (N) and VEGF mRNA expression (O) 2 d after transfection with HIF1α siRNA or control scrambled (Sble) siRNA, and then cultured for an additional 24 hr under 20% or < 1% oxygen tension in presence or absence of M&C; n = 3-6 experiments/group, SEM.

(P) Relative PGC1α (left) and VEGF (right) mRNA expression in HUVECs 2 d after transfection with PGC1α siRNA or control scrambled (Sble) siRNA and cultured in the indicated media for 16 hr; n = 3 experiments/group, SEM.

Unless otherwise indicated, error bars indicate SD; asterisks indicate the significance of the difference between SAA levels or genetic interventions by Student's t test; or between SAA levels within genotype/intervention/condition by one-way ANOVA with Sidak's multiple comparisons test; *$p < 0.05$, **$p < 0.01$, ***$p < 0.001$.

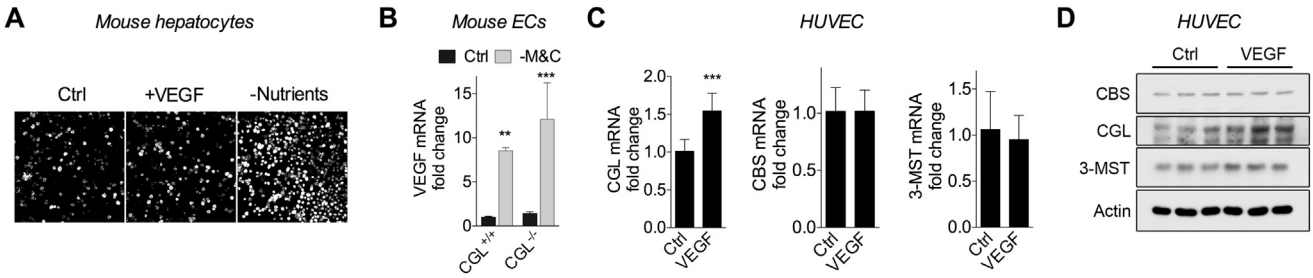

Figure S3. VEGF Signaling and AASR Converge on Endothelial H_2S Production by CGL, Related to Figure 3

(A) Representative images (10X mag) of H_2S-specific probe (P3) fluorescence in primary mouse hepatocytes treated with VEGF (50ng/ml) or deprived of all AAs as well as serum (-Nutrients) for 16 hr.

(B) VEGF mRNA in WT and CGLKO primary mouse ECs (n = 3 mice/group) cultured in M&C deficient media relative to control (Ctrl) media for 16 hr; error bars indicate SD; one-way ANOVA with Sidak's multiple comparisons test between SAA levels.

(C and D) CBS, CGL and 3-MST mRNA expression (C) and protein level (D) in HUVEC 16 hr after treatment with VEGF; n = 3 experiments/group, error bars indicate SEM; Student's t test. $^{**}p < 0.01$, $^{***}p < 0.001$.

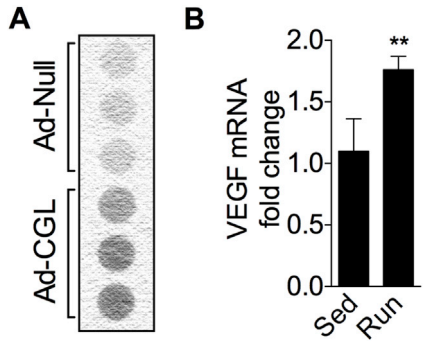

Figure S4. CGL Required for Angiogenesis *In Vivo*, Related to Figure 4

(A) H_2S production capacity of gastrocnemius muscle extracts of Ad Null or Ad-CGL infected mice 1 wk after the final intramuscular injection.

(B) Expression of VEGF mRNA in the gastrocnemius muscle of mice subjected to low-intensity exercise (Run) versus sedentary controls (Sed) for 1 mo; n = 4 mice/group.

Error bars indicate SD; asterisks indicate the significance of the difference between exercise groups by Student's t test; $^{**}p < 0.01$.

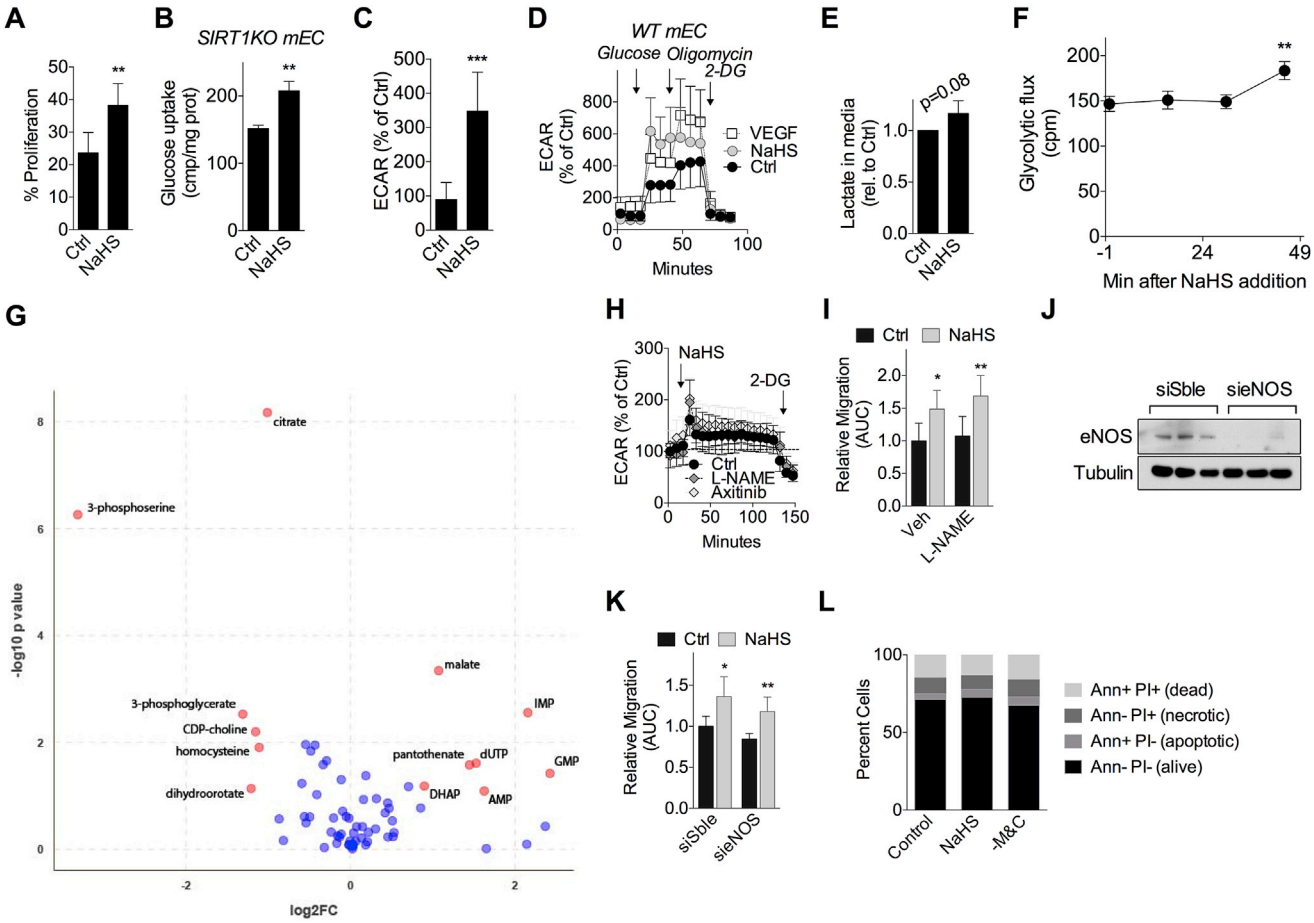

Figure S5. H_2S Promotes Glucose Uptake and ATP Generation by Glycolysis for EC Migration, Related to Figure 5

(A) HUVEC proliferation over a 24 hr period ± NaHS (100 μM) as assessed by radiolabelled thymidine incorporation; n = 5-9 experiments/group, error bars indicate SEM.

(B) Glucose uptake in SIRT1KO primary mouse ECs treated in triplicate as indicated.

(C) Extracellular acidification rate (ECAR) in HUVECs pretreated for 2 hr with NaHS (100 μM); n = 8 technical replicates from each of 2 experiments.

(D) ECAR over time in mouse ECs pretreated for 2 hr with VEGF (50 ng/ml) or NaHS (100 μM) and then treated with 10 mM Glucose, 2.5 μM Oligomycin and 50 mM 2-DG injection as indicated by the arrows; representative experiment shown.

(E) Fold change of lactate concentration in the media of HUVECs treated with NaHS (100 μM) for 1.5-6 hr versus control; n = 3 experiments per group; SEM.

(F) Glycolytic flux in HUVECs at the indicated time after NaHS addition; n = 3 technical replicates/time point; one-way ANOVA with Dunnett's multiple comparisons test versus t = 0.

(G) Log2 fold change of unlabeled metabolites in HUVECs treated for 1 hr with NaHS (100 μM) versus control.

(H) ECAR over time in HUVECs pre-treated for 2 hr with axitinib (10 μM) or L-NAME (100 μM) and then treated with NaHS or 2-DG as indicated by the arrows; n = 15 technical replicates/time point.

(I) Quantification of HUVEC migration across scratch ± NaHS (100 μM) or eNOS inhibitor L-NAME (100 μM); n = 5-6 AUC values/group each from cells at different passage numbers.

(J) Immunoblot of eNOS in HUVECs 2 d after transfection with eNOS siRNA or control scramble (Sble) siRNA.

(K) Quantification of HUVEC migration across scratch 2 d after transfection with eNOS siRNA or control scramble (Sble) siRNA ± NaHS (100 μM) as indicated; n = 6 AUC values/group each from cells at different passage number.

(L) Gating percentages based on annexin V (Ann) and propidium iodide (PI) stains in HUVECs treated with NaHS (100 μM) or –M&C for 12 hr.

Unless otherwise indicated, error bars indicate SD and asterisks indicate the significance of the difference between SAA levels by Student's t test or between SAA levels within genotype/condition by one-way ANOVA with Sidak's multiple comparisons test; *p < 0.05, **p < 0.01, ***p < 0.001.

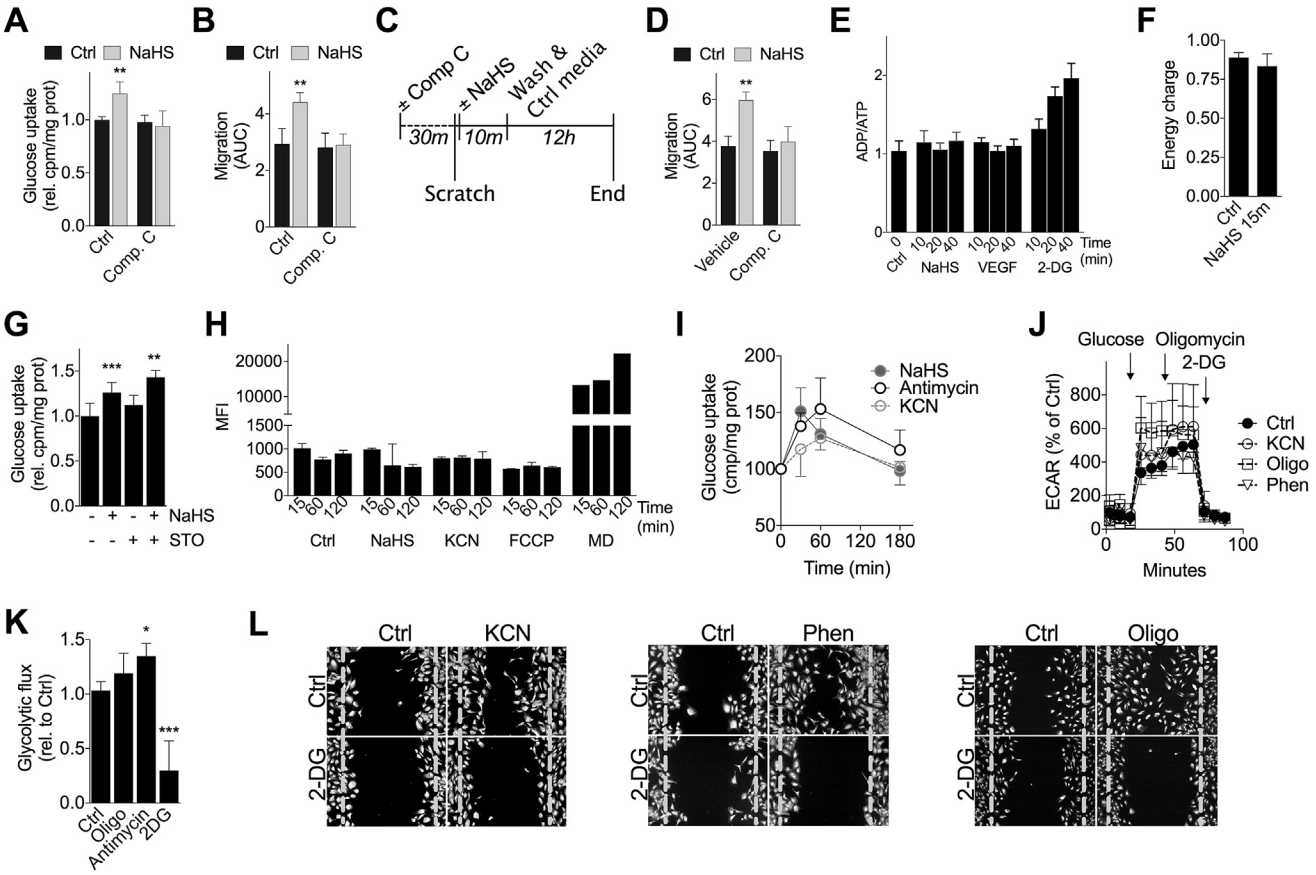

Figure S6. H_2S Shifts Oxidative/Glycolytic Balance Concomitant with Inhibition of Mitochondrial OXPHOS, Related to Figure 6

(A) Glucose uptake in HUVECs treated with NaHS for 1 hr ± 10 μM Compound C (Comp C); n = 6 experiments/group, error bars indicate SEM; one-way ANOVA with Sidak's multiple comparisons test between ± NaHS within Comp C treatment group.

(B) Migration across scratch in HUVECs treated with NaHS ± Comp C; n = 6 AUC values/group each from cells at different passage number; one-way ANOVA with Sidak's multiple comparisons test between ± NaHS within Comp C treatment group.

(C and D) Schematic of the experiment (C) and quantification of migration across scratch (D) in HUVECs treated with NaHS for 10 min in the presence of vehicle or Comp C; n = 5-6 AUC values/group each from cells at different passage number; one-way ANOVA with Sidak's multiple comparisons test between ± NaHS within Comp C treatment group.

(E) ATP/ATP ratio over time in HUVECs treated with the indicated compounds; representative of 2 experiements; n = 4-12 values/time point.

(F) Energy charge calculated from ATP, ADP and AMP measurements by mass spec in HUVECs treated for 15 min with NaHS; n = 6 values pooled fro 2 independent experiments; Student's t test.

(G) Glucose uptake in HUVECs treated with NaHS or the CamKKβ inhibitor STO-609; n = 3-9 values pooled from 2 independent experiments; one-way ANOVA with Sidak's multiple comparisons test between control and NaHS within STO or vehicle treatement group.

(H) ROS levels expressed as mean fluorescent intensity (MFI) in HUVECs treated over time with NaHS (100 μM), KCN (10 μM), FCCP (2 μM) or menadione (MD, 10 μM) as indicated; n = 2 values/time point.

(I) Time dependent glucose uptake in HUVEC treated with NaHS, KCN or antimycin as indicated; each time point is in triplicate.

(J) Extracellular acidification rate (ECAR) over time in HUVECs pretreated for 2 hr with 10 μM cyanide (KCN), 2 μM oligomycin (Oligo) or 500 μM phenformin (Phen) and then treated with 10 mM glucose, 2.5 μM oligomycin and 50 mM 2-DG as indicated by the arrows; n = 20 technical replicates pooled from 2 independent experiments.

(K) Glycolytic flux in HUVECS pretreated for 1-3 hr with oligomycin, antimycin A or 2-DG as indicated; n = 2-6 experiments/group; one-way ANOVA with Dunnett's multiple comparisons test relative to control.

(L) Representative images of migration across a scratch (10X mag at t = 20 hr; dotted lines indicate boundary of the scratch at t = 0 hr) from HUVECs cultured in the presence of 10 μM KCN (left), 500 μM phenformin (Phen, middle) or 2 μM oligomycin (Oligo, right) +/−1 mM 2-DG as indicated.

Unless otherwise noted, error bars indicate SD; *p < 0.05, **p < 0.01, ***p < 0.001.